

NJC

Accepted Manuscript



This article can be cited before page numbers have been issued, to do this please use: G. Devagi, F. Reyhaneh, F. Dallemer, R. Jayakumar, K. Palaniappan and R. Prabhakaran, *New J. Chem.*, 2017, DOI: 10.1039/C7NJ01707C.



This is an Accepted Manuscript, which has been through the Royal Society of Chemistry peer review process and has been accepted for publication.

Accepted Manuscripts are published online shortly after acceptance, before technical editing, formatting and proof reading. Using this free service, authors can make their results available to the community, in citable form, before we publish the edited article. We will replace this Accepted Manuscript with the edited and formatted Advance Article as soon as it is available.

You can find more information about Accepted Manuscripts in the [author guidelines](#).

Please note that technical editing may introduce minor changes to the text and/or graphics, which may alter content. The journal's standard [Terms & Conditions](#) and the ethical guidelines, outlined in our [author and reviewer resource centre](#), still apply. In no event shall the Royal Society of Chemistry be held responsible for any errors or omissions in this Accepted Manuscript or any consequences arising from the use of any information it contains.

Morphological and *in vitro* evaluation of programmed cell death in MCF-7 cells by new organoruthenium(II) complexes

G. Devagi^a, F. Reyhaneh^b, F. Dallemer^c, R. Jayakumar^b, P. Kalaivani^d, R. Prabhakaran^{a*}

^aDepartment of Chemistry, Bharathiar University, Coimbatore 641 046, India

^bDepartment of Molecular Medicine, University of Malaya, Kuala Lumpur 50603, Malaysia

^cLab MADIREL CNRS UMR 7246, Aix Marseille University, Saint-Jerome Campus, MADIREL Bldg., 13397 Marseille Cedex 20, France

^dDepartment of Chemistry, Nirmala College for Women, Bharathiar University, Coimbatore 641018

Abstract

Cyclopentadienylruthenium(II) thiosemicarbazone complexes, with the general formula $[\text{Ru}(\eta^5\text{-C}_5\text{H}_5)(\text{Ac-tsc})\text{PPh}_3]\cdot\text{Cl}$ (**1**), $[\text{Ru}(\eta^5\text{-C}_5\text{H}_5)(\text{Ac-mtsc})\text{PPh}_3]\cdot\text{Cl}$ (**2**), $[\text{Ru}(\eta^5\text{-C}_5\text{H}_5)(\text{Ac-etsc})\text{PPh}_3]\cdot\text{Cl}$ (**3**) and $[\text{Ru}(\eta^5\text{-C}_5\text{H}_5)(\text{Ac-ptsc})\text{PPh}_3]$ (**4**) were synthesized and characterized by various spectroscopic techniques (¹H-NMR, ¹³C-NMR, IR and UV-Vis). The molecular structure of representative complexes **2** and **4** was studied by single crystal X-Ray diffraction. Interaction of all the ligands and complexes with Calf Thymus-DNA (CT-DNA) and Bovine Serum Albumin (BSA) was studied using UV-Vis and Fluorescence emission spectroscopy, the results of the binding studies cleared that the effective binding potential of the complexes are higher than their parent ligands. All the new complexes (**1-4**) were evaluated for their *in vitro* cytotoxic activity against MCF-7 cancer cell line. All the complexes significantly inhibited cell proliferation in human MCF-7 breast cancer cells in a dose-dependent manner. Cytological observations by an inverted phase contrast microscope and Hoechst 33342/PI dual-staining assay showed typical apoptotic morphology of cancer cells upon treatment with complexes **2** and **3**. It can thus be suggested that complexes **2** and **3** are modulated by apoptosis. The findings of the present study support that the complexes **2** and **3** can be of potent drugs for the treatment of cancer related diseases only after further explorations.

Keywords: Organoruthenium(II) complexes, CT-DNA, Bovine Serum Albumin, Ethidium Bromide, Anticancer activity, Apoptosis and Morphology

Corresponding author Tel.: +91-422-2428319; Fax: +91-422-2422387.

E-mail address: rpnchemist@gmail.com (R. Prabhakaran)

Introduction

There is considerable interest in metal based chemotherapeutic studies and number of evidence demonstrating that metal-based compounds are promising candidates for cancer treatments. For instance, complexes possessing platinum, such as cisplatin, carboplatin and oxaliplatin, have been used to treat several cancer types such as ovary, stomach, and colon.^{1,2} The mechanism of cancer cell growth inhibition by platinum complexes achieved by causing inter and intra-strand cross-linking with DNA, thus preventing DNA repair or replication.³ However, former studies confirmed that platinum complexes have severe side effects and generate resistant to cancer cells, limiting the efficacy of these complexes in clinical trials.⁴ However, metal based complexes are the promising anti-cancer drugs due to their ease of chemical modification and wide-spectrum of effectiveness against various origins of cancer. Ruthenium complexes are potent growth inhibitors for many cancer cells such as ovarian, melanoma, and breast.⁵⁻¹⁰ They have been used as an alternative to platinum complexes for development of novel anti-cancer drugs with less or no side effects. Certainly, several ruthenium complexes are under phase I or II clinical trials.¹¹⁻¹³ Based on the structure-activity relationship studies (SARS), ruthenium complexes may function to inhibit tumor cells through mechanisms similar to that of *cisplatin*.¹⁴ Some ruthenium(III) complexes (NAMIA, KP1019 and KP1330) are in Phase II clinical trials.¹⁵ In addition, other organometallic ruthenium (II) arene complexes, RM175 and RAPTA complexes, have also shown promising activity.^{16,17} The nature of the ligands bound to the metal ion is important for the activity of the drug. Thus we chose thiosemicarbazide ligands, further they are a class of Schiff base compounds showed different molecular geometry with metal complexes and are familiar for their biological activity as antiparasitics, antibacterial, antifungal, antiviral, and antitumoral agents.¹⁸ Cellular homeostasis is conserved *via* a tightly controlled apoptotic (programmed cell death) mechanism.^{19, 20} This is attained *via* two major pathways—the extrinsic pathway that occurs through death receptors present in the outer membrane of the cell, and the intrinsic pathway, which is a mitochondria-dependent pathway.²¹ Critical defect in the apoptotic signalling pathways may lead to uncontrolled proliferation and cell growth which may ultimately lead to cancer, and the use of chemotherapeutic agents to induce apoptosis in cancer is one of the effective ways to overcome this deadly disease. The connection between apoptosis and cancer has been highlighted, with increasing evidence suggesting that the linked processes of neoplastic transformation, progression and metastasis involve the change of normal apoptotic pathways.²² Apoptosis afforded a number of hints

with respect to effective anticancer therapy, and numerous chemotherapeutic agents reportedly exert their antitumor effects by inducing apoptosis in cancer cells.²³ Apoptosis not only plays an important role in the development and maintenance of tissue homeostasis, but it also represents an active mechanism by which harmful cells can be removed.^{23,24} Typical morphological types of apoptotic cells can be witnessed through microscopic studies using the inverted phase contrast and fluorescence microscope. Other features such as chromatin condensation and nuclear fragmentation can be better observed through the double staining with Hoechst 33342 and propidium iodide using fluorescence microscopic analysis. This is a convenient and rapid assay, widely used to identify live and dead cells. Hoechst 33342 is a blue fluorescing dye that stains chromatin DNA. The red fluorescing dye propidium iodide is only permeable to dead cells and cannot enter the intact plasma membrane of living cells. Thus, the staining pattern resulted from the simultaneous use of these dyes make it possible to distinguish normal, apoptotic, and dead cells population by fluorescence microscopy.²⁵⁻²⁸ Also, it is highly desirable to have compounds that can cause cancer cell death via apoptosis. Herein, the present study focused on synthesis and characterisation of new cyclopentadienylruthenium(II) complexes and their cytotoxicity on human cancer cell line, namely, the hormone-dependent breast cancer cell line (MCF-7). The presence of apoptosis induced by complexes was then investigated through morphological observation of the cancer cells using inverted phase contrast and fluorescence microscope (Hoechst 33342/PI). Further, the apoptosis was confirmed with flow cytometry (Annexin V-FITC).

Measurements

Melting points were measured in a Lab India apparatus. Infrared spectra were measured as KBr pellets on a Jasco FT-IR 400- 4100 cm^{-1} range. Elemental analyses of carbon, hydrogen, nitrogen and sulfur were determined by using Vario EL III CHNS at the Department of Chemistry, Bharathiar University, Coimbatore, India. (TMS). Electronic absorption spectra of the ligands and complexes were recorded using JASCO 600 spectrophotometer and emission measurements were carried out by using a JASCO FP-6600 spectrofluorometer. ^1H and ^{13}C NMR spectra were recorded in CDCl_3 at room temperature with a Bruker 400 MHz instrument, chemical shift relative to tetramethylsilane. The chemical shifts are expressed in parts per million (ppm). CT-DNA, pBR322 plasmid DNA, BSA and ethidium bromide (EB) were obtained from Himedia. Single crystal data collections and corrections for the new Ru(II) complexes **2** and **4** were done at 293 K with CCD Kappa Diffractometer using graphite mono chromated Mo Ka ($k = 0.71073 \text{ \AA}$) radiation.²⁹ The

structural solutions were done by using SHELXS-97³⁰ and refined by full matrix least square on *F*² using SHELXL-2014.³¹

EXPERIMENTAL SECTION

All the reagents used were analar grade, were purified and dried according to the standard procedure.³² The ligands (**HL**¹⁻⁴) and the ruthenium complex [RuCl(PPh₃)₂(η⁵-C₅H₅)] were synthesized according to the standard literature procedures.³³⁻³⁵

General Procedure for the Synthesis of ligands.

Preparation of acetone-thiosemicarbazone.[H-Ac-tsc](**HL**¹).

Thiosemicarbazide (1 mmol) and acetone (1 mmol) were combined in methanol (5 mL) with acetic acid (1–2 drops). The mixture was refluxed for 3 h, during which a white precipitate appeared. After 3 h, the mixture was allowed to cool to room temperature, and dried *in vacuo*. Ligands were further purified by recrystallization from methanol. Yield: 89 %. Mp 162 °C. Anal. calcd for C₄H₉N₃S: C, 36.62; H, 6.91; N, 32.03; S, 24.44. Found: C, 36.59; H, 6.88; N, 32.01; S, 24.40 %. FT-IR (cm⁻¹) in KBr: 1596 (ν_{C=N}), 863 (ν_{C=S}); ¹H NMR (CDCl₃, ppm): δ 1.92 (s, 3H, -C(CH₃)₂), δ 2.01 (s, 3H, -C(CH₃)₂), δ 8.57 (s, 1H, -NH-C=S), δ 6.44 (s, 2H, terminal -NH₂).

A similar method was followed to prepare other ligands.

Preparation of acetone-4(*N*)-methylthiosemicarbazone. [H-Ac-mtsc](**HL**²).

Ligand **HL**² was prepared by the procedure as described for (**HL**¹) with 4(*N*)-methylthiosemicarbazide. Yield: 91 %. Mp 95 °C. Anal. calcd for C₅H₁₁N₃S: C, 41.35; H, 7.63; N, 28.93; S, 22.08. Found: C, 41.30; H, 7.65; N, 28.89; S, 22.11 %. FT-IR (cm⁻¹) in KBr: 1556 (ν_{C=N}), 850 (ν_{C=S}); ¹H NMR (CDCl₃, ppm): δ 1.88 (s, 3H, -C(CH₃)₂), δ 1.99 (s, 3H, -C(CH₃)₂), δ 8.38 (s, 1H, -NH-C=S), δ 7.50-7.52 (d, 1H, J = 8 Hz, terminal -NH), δ 3.20-3.21 (d, 3H, J = 4 Hz, terminal -CH₃).

Preparation of acetone-4(*N*)-ethylthiosemicarbazone.[H-Ac-etsc](**HL**³).

Ligand **HL**³ was prepared by the procedure as described for (**HL**¹) with 4(*N*)-ethylthiosemicarbazide. Yield: 85 %. Mp 63 °C. Anal. calcd for C₆H₁₃N₃S: C, 45.25; H, 8.23; N, 26.39; S, 20.13. Found: C, 45.19; H, 8.20; N, 26.31; S, 20.09 %. FT-IR (cm⁻¹) in KBr: 1637 (ν_{C=N}), 829 (ν_{C=S}); ¹H NMR (CDCl₃, ppm): δ 1.89 (s, 3H, -C(CH₃)₂), δ 2.00 (s, 3H, -C(CH₃)₂), δ 8.39 (s, 1H, -NH-C=S), δ 7.47-7.53 (d, 1H, J = 24 Hz, terminal -NH), δ 3.20-3.21 (d, 3H, J = 4 Hz, terminal methylene protons), δ 3.16-3.17 (d, 3H, J = 4 Hz, terminal methyl protons).

Preparation of acetone-4(*N*)-phenylthiosemicarbazone.[H-Ac-ptsc](HL⁴).

Ligand HL⁴ was prepared by the procedure as described for (HL¹) with 4(*N*)-ethylthiosemicarbazide. Yield: 92 %. Mp 114 °C. Anal. calcd for C₁₀H₁₃N₃S: C, 57.94; H, 6.32; N, 20.27; S, 15.47. Found: C, 57.91; H, 6.28; N, 20.22; S, 15.45 %. FT-IR (cm⁻¹) in KBr: 1592 (ν_{C=N}), 826 (ν_{C=S}); ¹H NMR (CDCl₃, ppm): δ 1.94 (s, 3H, -C(CH₃)₂), δ 2.05 (s, 3H, -C(CH₃)₂), δ 9.28 (s, 1H, -NH-C=S), δ 8.58 (s, 1H, terminal -NH), δ 7.18-7.20 (t, 1H, J= 8 Hz, terminal phenyl proton), δ 7.35-7.38 (t, 2H, J= 7.2 Hz, terminal phenyl protons), δ 7.660-7.663 (d, 2H, J= 1.2 Hz, terminal phenyl protons).

Synthesis of new Ruthenium(II) complexes**Synthesis of [RuCp(Ac-tsc)(PPh₃)]·Cl (1).**

To a solution of [RuCl(PPh₃)₂(η⁵-C₅H₅)] (0.20 g, 0.2752 mmol) in methanol (10 cm³), acetone-4(*N*)-phenylthiosemicarbazone [H-Ac-tsc] (0.036 g, 0.2752 mmol) in methanol (10 cm³) was added. The reaction mixture was then refluxed for 5 h. The reddish orange suspension gradually turned to red color. The solvent was removed under reduced pressure. The orange solid formed was washed with petroleum ether (60-80°C) 2-3 times. The complex was crystallized from CHCl₃/ n-heptane. Yield: 69 %. Mp 112 °C. Anal. calcd for C₂₇H₂₉ClN₃PRuS: C, 54.49; H, 4.91; N, 7.06; S, 5.39. Found: C, 54.52; H, 4.89; N, 7.04; S, 5.37 %. FT-IR (cm⁻¹) in KBr: 1599 (ν_{C=N}), 839 (ν_{C=S}); UV-Vis (CH₂Cl₂), λ_{max}: 242 (140,352) nm (dm³ mol⁻¹cm⁻¹) (intra-ligand transition) and 321 (45,752) nm (dm³ mol⁻¹cm⁻¹) (LMCT); ¹H NMR (CDCl₃, ppm): δ 2.10 (s, 3H, -C(CH₃)₂), δ 2.29 (s, 3H, -C(CH₃)₂), δ 4.37 (s, 5H, -Cp protons), δ 12.51 (s, 1H, -NH-C=S), δ 9.35 (s, 2H, terminal -NH₂), δ 7.15-7.69 (m, 15H, triphenylphosphine(aromatic region)). ¹³C NMR (CDCl₃, ppm): δ 180.83 (C=S), δ 166.96 (C=N), δ 78.12 (Cp), δ 22.36 (C(CH₃)₂), δ 128.30-135.49 (aromatic PPh₃).

A similar method was followed to synthesize other complexes.

Synthesis of [RuCp(Ac-mtsc)(PPh₃)]·Cl (2).

Complex 2 was prepared by the procedure as described for (1) with acetone-4(*N*)-methylthiosemicarbazone [H-Ac-mtsc] (0.039 g, 0.2752mmol). Orange solid formed was washed with petroleum ether (60–80°C). The complex was crystallized from CHCl₃/ n-heptane. Yield: 71 %. Mp 101 °C. Anal. calcd for C₂₈H₃₁ClN₃PRuS: C, 55.21; H, 5.13; N, 6.90; S, 5.26. Found: C, 55.19; H, 5.09; N, 6.87; S, 5.29 %. FT-IR (cm⁻¹) in KBr: 1580 (ν_{C=N}), 837 (ν_{C=S}); UV-Vis (CH₂Cl₂), λ_{max}: 255 (216,963) nm (dm³ mol⁻¹cm⁻¹) (intra-ligand transition) and 317 (118,229) nm (dm³ mol⁻¹cm⁻¹) (LMCT); ¹H NMR (CDCl₃, ppm): δ 2.09

(s, 3H, -C(CH₃)₂), δ 2.25 (s, 3H, -C(CH₃)₂), δ 4.35 (s, 5H, -Cp protons), δ 12.08 (s, 1H, -NH-C=S), δ 9.72 (s, 1H, , terminal -NH), δ 3.007-3.019 (d, 3H, J= 4.8 Hz, terminal -CH₃), δ 7.15-7.41 (m, 15H, triphenylphosphine(aromatic region)). ¹³C NMR (CDCl₃, ppm): δ 182.12 (C=S), δ 173.10 (C=N), δ 83.66 (Cp), δ 26.40 (C(CH₃)₂), δ 31.30 (NH-CH₃), δ 128.03-133.37 (aromatic PPh₃).

Synthesis of [RuCp(Ac-etsc)(PPh₃)]Cl (3).

Complex **3** was prepared by the procedure as described for (**1**) with acetone-4(*N*)-ethylthiosemicarbazone [H-Ac-etsc] (0.040 g, 0.2752 mmol). Reddish orange solid formed was washed with petroleum ether (60–80°C). The complex was crystallized from CHCl₃/ *n*-heptane. Yield: 73 %. Mp 92 °C. Anal. calcd for C₂₉H₃₃ClN₃PRuS: C, 55.89; H, 5.34; N, 6.74; S, 5.15. Found: C, 55.92; H, 5.30; N, 6.73; S, 5.09 %. FT-IR (cm⁻¹) in KBr: 1571 ($\nu_{C=N}$), 841 ($\nu_{C=S}$); UV-Vis (CH₂Cl₂), λ_{max} : 254 (214,398) nm (dm³ mol⁻¹cm⁻¹) (intra-ligand transition) and 309 (106,424) nm (dm³ mol⁻¹cm⁻¹) (LMCT); ¹H NMR (CDCl₃, ppm): δ 2.10 (s, 3H, -C(CH₃)₂), δ 2.25 (s, 3H, -C(CH₃)₂), δ 4.36 (s, 5H, -Cp protons), δ 12.03 (s, 1H, -NH-C=S), δ 9.78 (s, 1H, , terminal -NH), δ 3.42-3.50 (m, 2H, J= 4 Hz, terminal methylene protons), δ 1.206-1.242 (t, 3H, J= 7.2 Hz, terminal -CH₃), δ 7.17-7.37 (m, 15H, triphenylphosphine(aromatic region)). ¹³C NMR (CDCl₃, ppm): δ 179.66 (C=S), δ 164.60 (C=N), δ 82.16 (Cp), δ 22.27 (C(CH₃)₂), δ 39.99 (NH-CH₂), δ 32.45 (NHCH₂-CH₃), δ 128.23-135.62 (aromatic PPh₃).

Synthesis of [RuCp(Ac-ptsc)(PPh₃)] (4).

Complex **4** was prepared by the procedure as described for (**1**) with acetone-4(*N*)-phenylthiosemicarbazone [H-Ac-ptsc] (0.056 g, 0.2752mmol). Orange solid formed was washed with petroleum ether (60–80°C). The complex was crystallized from chloroform and *n*-heptane. Yield: 69 %. Mp 107 °C. Anal. calcd for C₃₃H₃₂N₃PRuS: C, 62.44; H, 5.08; N, 6.62; S, 5.05. Found: C, 62.39; H, 5.05; N, 6.58; S, 4.99 %. FT-IR (cm⁻¹) in KBr: 1539 ($\nu_{C=N}$), 740 (ν_{C-S}); UV-Vis (CH₂Cl₂), λ_{max} : 264 (234,923) nm (dm³ mol⁻¹cm⁻¹), 295 (240,650) nm (dm³mol⁻¹cm⁻¹) (intra-ligand transition) and 349 (108,653) nm (dm³ mol⁻¹cm⁻¹) (LMCT); ¹H NMR (CDCl₃, ppm): δ 2.00 (s, 3H, -C(CH₃)₂), δ 2.30 (s, 3H, -C(CH₃)₂), δ 4.31 (s, 5H, -Cp protons), δ 5.29 (s, 1H, terminal -NH), δ 6.72-7.417 (m, 20H, phenyl protons and triphenylphosphine(aromatic region)). ¹³C NMR (CDCl₃, ppm): δ 176.31 (C=S), δ 170.21 (C=N), δ 81.12 (Cp), δ 22.72 (C(CH₃)₂), δ 122.57-133.14 (aromatic and PPh₃).

Binding studies

Various concentration (5–50 μM) of Calf thymus DNA (CT DNA) were prepared by dissolving in TrisHCl buffer with pH equal to 7.2. The Absorption spectra was recorded in a JASCO spectrophotometer with 1 cm path length of the cuvettes after equilibrium attained at 20 $^{\circ}\text{C}$ for 10 min. The binding titration experiment has been carried out by fixing the complex concentration as constant and by varying the DNA concentration. The absorbance intensity (A) for each complex was recorded after the addition of DNA to the complexes.

Ethidium Bromide Displacement Assay

Emission intensity measurements were carried out by using a 5% DMF/ 5 mMTris-HCl/ 50 mMNaCl buffer solution as a blank to make preliminary adjustments. The excitation wavelength was fixed and the emission range was adjusted before measurements. DNA was pre-treated with EB in the ratio $[\text{DNA}/\text{EB}] = 10$ for 30 min at 27 $^{\circ}\text{C}$. The metal complexes were then added to this mixture, and their effect on the emission intensity was measured.

DNA Cleavage study

The cleavage of DNA was checked using agarose gel electrophoresis. Supercoiled pBR322 DNA (100 ng) in 5% DMSO and 95% Tris buffer (5 mM, pH 7.2) with 50 mMNaCl was incubated at 37 $^{\circ}\text{C}$ in the absence and presence of compounds (50 μM). The DNA, compound, and sufficient buffer were premixed in a vial, and the reaction was allowed to proceed for 2 h at 37 $^{\circ}\text{C}$ before the addition of ethylene glycol and loading onto an agarose gel. Agarose gel electrophoresis of plasmid DNA was performed at 50 V in 1% slab gels containing 0.5 $\mu\text{g mL}^{-1}$ ethidium bromide in Tris buffer. DNA was visualized by photographing the fluorescence of intercalated ethidium bromide under a UV illuminator. The cleavage efficiency was measured by determining the ability of the compounds to convert the supercoiled (SC) DNA to the nicked circular (NC) form and linear circular (LC) form. After that the gel was documented on a Digital Gel Documentation system unit (Syngene, USA).

BSA binding experiments

The protein binding study was performed by tryptophan fluorescence quenching experiments using bovine serum albumin (BSA, 10 μM) as the substrate in phosphate buffer (pH 6.8). Quenching of the emission intensity of tryptophan residues of BSA at 347-349 nm (excitation wavelength at 280 nm) was monitored using ligands (HL^1 - HL^4) and complexes **1–4** as quenchers with increasing complex concentration. The excitation and emission slit

widths were 5 and 10 nm, respectively. Fluorescence measurements were performed using a 1 cm quartz cell on a JASCO F6500 spectrofluorimeter.

HSA-binding experiments

The protein binding study was performed by tryptophan fluorescence quenching experiments using human serum albumin (HSA, 10 μ M) as the substrate in tris-Hcl buffer (pH 7.2). A 3.0 mL portion of aqueous solution of HSA (10 μ M) was titrated by successive additions of the ligands (**HL**¹-**HL**⁴) and complexes **1**-**4**. For every addition, the mixture solution was shaken and allowed to stand for 10 min, and then the fluorescence intensities were measured with the excitation and emission wavelength set at 280 nm and 300–500 nm, respectively. In the meantime, the synchronous fluorescence intensity of the mixture solution was measured at $\Delta\lambda = 60$ nm and $\Delta\lambda = 15$ nm, respectively. For fluorescence enhancement experiments, the Ru(II) complex (10 μ M) in 0.05 M Tris-HCl/0.15 M NaCl buffer of pH 7.2 was titrated with HSA. The fluorescence emission spectrum was recorded in the wavelength range of 310–600 nm with an excitation wavelength of 300 nm.

In vitro evaluation of anticancer activity

Cell viability.

The 3-(4,5-dimethylthiazol-2-yl)-2,5-diphenyltetrazolium bromide (MTT) assay is a quantitative, sensitive and reliable colorimetric assay generally used for assessing viability and proliferation of the cells. In this assay mitochondrial dehydrogenase enzymes of live cells convert the yellow water soluble substrate, MTT into a purple formazan crystal product which is insoluble in water or medium.³⁶

The cytotoxic potential of the compounds were assessed using a colorimetric MTT reduction assay using MCF-7 breast cancer cells and HaCaT(human immortalized, but 'non-cancerous') cells. Briefly, cells were seeded in a 96-well flat bottom transparent plate at a concentration of 7×10^3 and incubated for 24 hours at 37 °C in an incubator supplied with 5% CO₂. After 24 hours, the cells were treated with different concentrations of compounds (3.12, 6.25, 12.5, 25, 50, 100 and 200 μ g/mL) and 0.1% DMSO was used as a vehicle control and incubated for 24 h. After the incubation, a 50 μ l of MTT solution (2 mg/mL in phosphate-buffered saline) was added to each well and the plate was incubated for an additional 2h. Then the supernatant in each well was removed and 100 μ L of DMSO was added to dissolve the produced formazan crystal. Plates were then shaken for 15 min at room temperature for complete solubilization. The absorbance was measured at 570 nm using a Tecan infinite M1000Pro microplate reader (Tecan, Männedorf, Switzerland). The assay was performed in

triplicate in 3 independent studies and the concentration of complexes with 50% reduction in cellular viability was expressed as the half maximal inhibitory concentration (IC_{50}) value.

Morphological changes of nucleus with Hoechst 33342/PI Staining

Cell death is discriminated into two main forms, apoptosis and necrosis. In contrast to necrosis, apoptosis is a programmed and regulated pathway of cell death.³⁷ Morphological hallmarks of apoptosis in the nucleus are chromatin condensation and nuclear fragmentation.³⁸ This condensation and fragmentation can be followed by fluorescence microscopy after staining with DNA binding fluorescence dyes. Hoechst and PI double staining provide a fast and suitable assay for nucleus morphology and apoptosis. Hoechst binds in the minor groove of double stranded DNA preferably AT rich region while PI intercalates between the bases without any sequence preference. PI is normally used to identify dead cells as it is membrane impermeable and gets excluded from viable cells while Hoechst dye is permeable to the cell membrane and binds to DNA in live or fixed cells.

For this experiment, 8×10^4 MCF-7 cells were seeded into a 24-well plate. After incubation, cells were treated with or without tested compounds at IC_{50} concentration and further incubated for 24h at 37°C in an incubator supplied with 5% CO_2 . After incubation, the media was discarded and the cells were stained with Hoechst 33342 solution (10 $\mu\text{g/mL}$). The plate was further incubated for 10 min in the dark at 37°C. Then, the cells were counter stained with propidium iodide (2.5 $\mu\text{g/mL}$) for 5 min in the dark at room temperature and then fluorescence was imaged by fluorescence microscope at 100 \times magnifications.

Morphological Changes of MCF7 cells using phase contrast inverted microscope

Observation of morphological changes of apoptotic cells was performed according to the method with slight modifications.²⁵ Briefly, MCF-7 cells were seeded into 24-well plate and incubated overnight to attach. Then, the cells were treated with or without test compounds (control) at different concentrations of 3 $\mu\text{g/mL}$, 6 $\mu\text{g/mL}$ and 12 $\mu\text{g/mL}$ for complex **2** and 3.5 $\mu\text{g/mL}$, 7 $\mu\text{g/mL}$ and 14 $\mu\text{g/mL}$ for complex **3** was incubated 24h at 37°C with 5% CO_2 . The morphological changes of the cells were observed using an inverted light microscope at 100X magnification.

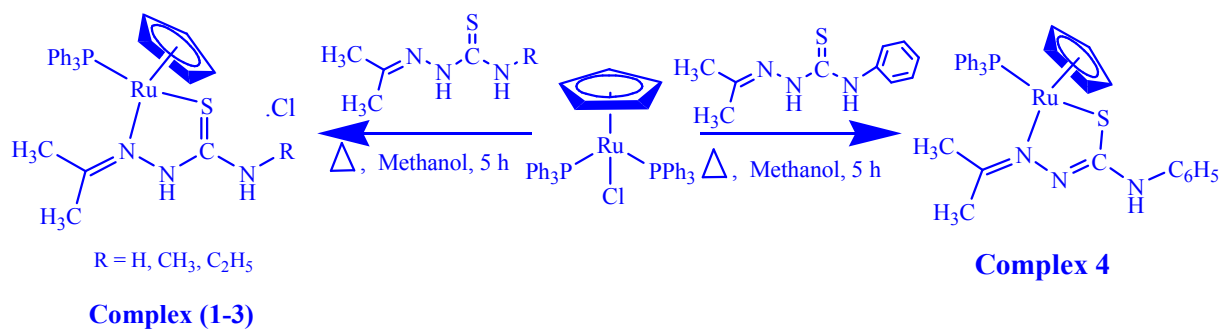
Annexin V/PI double stainig assay

The procedure was conducted with Annexin V-FITC Apoptosis Detection Kit (eBioscience, USA) according to manufacturer's protocol. Briefly, $2-5 \times 10^5$ cells were seeded in 6-well plate and incubated overnight. The cells were treated with complex **2** (6 $\mu\text{g/mL}$ and 12 $\mu\text{g/mL}$) and Complex **3** (7 $\mu\text{g/mL}$ and 14 $\mu\text{g/mL}$) compounds and incubated for

24 h at 37°C with 5% CO₂. Then, the treated cells were harvested, washed with PBS and resuspended in binding buffer. The cells were incubated for 10 minutes in dark with 5 µg/ml Annexin V-FITC in room temperature. After incubation, 10 µg/ml of PI was added to the cell suspension and the fluorescence of the cells were measured by flow cytometry system (FACs CANTO II).

Results and Discussion

The reactions of [RuCl(PPh₃)₂(η⁵-C₅H₅)] with an equimolar amount of various 4(*N*)-substituted thiosemicarbazones (HL¹–HL⁴) in methanol resulted in the formation of new complexes (**Scheme 1**), the analytical data of which confirmed the stoichiometry of the complexes (**1–4**). The structure of the complexes **2** and **4** were confirmed by X-ray crystallographic studies and attempts were made to grow single crystals of complex **1** and **3** in various organic solvents were unsuccessful. The complexes are soluble in common organic solvents such as dichloromethane, chloroform, benzene, acetonitrile, ethanol, methanol, dimethylformamide and dimethylsulfoxide.



Spectroscopic Studies

The IR and UV spectral details are given in the supporting information. The ¹H-NMR spectra of [HL¹-HL⁴] showed a singlet at δ 8.38-9.28 ppm corresponding to (N(2)H-C=S) group,³⁹ in the complexes **1-3**, a singlet occurred at δ 12.03-12.51 ppm due to (N(2)H-C=S) group indicating that the ligand remains in its thionic form.⁴⁰ This shift showed that the thiosemicarbazone is coordinated to the ruthenium through thione sulphur atom rather than thiolate sulphur.^{42,43} However, in complex **4** there was no resonance attributable to N(2)H, indicating coordination of the thiolate sulphur ligand in the anionic form after deprotonation at N(2). In complexes (**1-4**) a sharp singlet appeared at δ 4.31-4.37 ppm due to cyclopentadienyl protons.⁴⁴ A singlet observed in the ligand **HL**¹ at δ 6.44 ppm due to terminal (-NH₂) was appeared at 9.35 in the complex **1**.⁴⁰ A doublet observed in the ligands **HL**² and **HL**³ around δ 7.47-7.53 ppm due to terminal (-NH) was appeared in the complexes

2 and **3** as a singlet at δ 9.72 ppm and δ 9.78 ppm respectively. ⁴⁰Whereas, in **HL**⁴ and complex **4**, terminal (-NH) was observed as a singlet at δ 8.58 ppm and 5.29 ppm respectively. ⁴¹A doublet observed in the **HL**² and complex **2** at δ 3.00-3.21 ppm due to the presence of terminal methyl protons. For **HL**³ and complex **3** methylene protons of ethyl group appeared as a doublet at δ 3.20-3.50 ppm and methyl protons of ethyl group appeared at δ 1.20-3.17 ppm. ⁴⁵Two singlets for each ligands (**HL**¹-**HL**⁴) and complexes (**1-4**) observed at δ 1.88-2.05 and δ 2.1-2.3 ppm was due to methyl protons of acetone. ⁴⁰The ¹³C {¹H} NMR spectra of the complexes (**1-4**) contain resonances for the cyclopentadienyl ring carbons around δ 78.12-83.66 ppm. ⁴⁴The resonance observed around δ 164.60-173.10 ppm assigned to the (C=N) carbon of the ligands. ⁴²In complex **4**, thioliccarbon signal of the ligand was observed at δ 176.31 ppm whereas in the complexes (**1-3**) this signal was observed around 179.66-182.12 ppm as more deshielded indicating the thione sulphur coordination to ruthenium. ^{46,47}The spectra also showed resonance in the range of δ 122.57-135.62 ppm corresponding to the aromatic carbons. ⁴²In all the complexes resonances observed around δ 22.27-26.40 ppm was due to the methyl carbons of acetone group of ligand. In complex **2** a signal observed at δ 31.30 ppm has been assigned to terminal HN-CH₃ carbons. In complex **3**, signals observed at δ 39.99 ppm and δ 32.45 ppm were corresponding to the presence of methylene and methyl carbons of ethyl group. ⁴⁸The molar conductance for complex **1** and **3** was found to be 101 $\Omega^{-1}\text{cm}^2\text{mol}^{-1}$ and 109 $\Omega^{-1}\text{cm}^2\text{mol}^{-1}$ is found to be in agreement with 1:1 electrolytic behaviour. ⁴⁹

X-Ray Crystallographic studies

Complexes **2** and **4** crystallized in monoclinic space group P2₁/c (Fig. 1 and 2, Table 1). In complex **2**, the ligand [H-(Ac-mtsc)] (**HL**²) is coordinated to ruthenium ion through the N(3) nitrogen and thione sulphur atoms, forming a stable five member chelate ring with a bite angle [N(3)-Ru(1)-S(1)] of 81.04(8)°. The Ru(1)-N(3) and Ru(1)-S(1) distances found as 2.145(3) Å and 2.3651(10) Å respectively. The other sites are occupied by triphenylphosphine Ru(1)-P(1) distances of 2.310(10) Å and cyclopentadienyl ligand with Ru(1)-C(6), Ru(1)-C(7), Ru(1)-C(8) Ru(1)-C(9) Ru(1)-C(10) distance of 2.157(4), 2.200(4), 2.208(4), 2.202(4), 2.160(4) Å respectively. The observed bond distances are comparable with those found in other reported ruthenium complexes containing triphenylphosphine and cyclopentadiene. ⁵⁵In addition, complex **2** contains two intermolecular hydrogen bonding through the hydrogen atom of the terminal nitrogen(N1) with the chlorine atom(Cl2(A)) employing as charge compensating anion having N(1)-H(1)⋯Cl2(A) distance

of 3.180 Å and a hydrogen atom of the(N2) imine nitrogen with the chlorine atom(Cl2(A)) having N(2)–H(2)···Cl2(A) distance of 3.141 Å (Fig. S14). In complex **4**, the ligand [H-(Ac-ptsc)] (HL⁴) coordinated to ruthenium in NS fashion by utilizing its, N1 nitrogen, and thiolate sulphur atoms with the formation of stable five member ring with a bite angle N(1)–Ru(1)–S(1) of 80.36(6)°. The Ru(1)–N(1) and Ru(1)–S(1) distances found as 2.137(2) Å and 2.3522(7) Å respectively. The other site is occupied by triphenylphosphine with Ru(1)–P(1) distance of 2.2847(2) Å and a cyclopentadienyl ligand with Ru(1)–C(35), Ru(1)–C(36), Ru(1)–C(37), Ru(1)–C(38), Ru(1)–C(39) 2.157(3), 2.166(3), 2.204(3), 2.194(3), 2.197(3) Å respectively. The observed bond distances are comparable with those found in other reported ruthenium complexes containing triphenylphosphine and cyclopentadiene.⁵⁰The selected bond length and bond angles are given in **Table. 2**. Further, there were no greater variations observed in the bond lengths and bond angles of complex **2** and complex **4**.

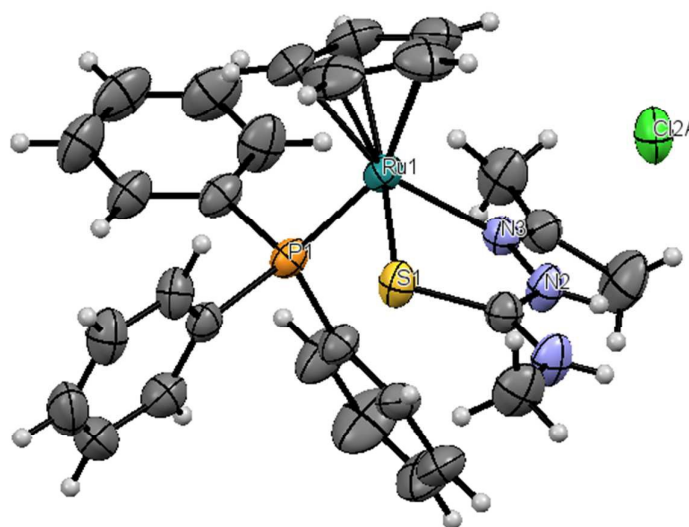


Fig. 1. ORTEP for [RuCp(Ac-mtsc)(PPh₃)]·Cl (**2**)

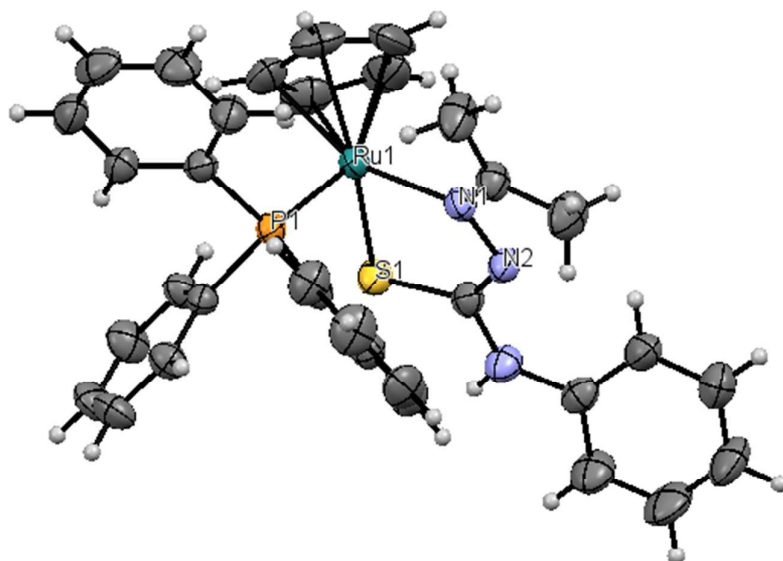


Fig. 2. ORTEP for [RuCp(Ac-ptsc)(PPh₃)] (4)

Table 1. Crystallographic data of complexes [RuCp(Ac-*mtsc*)(PPh₃)]·Cl (**2**) and [RuCp(Ac-*ptsc*)(PPh₃)] (**4**)

	[RuCp(Ac- <i>mtsc</i>)(PPh ₃)]·Cl (2)	[RuCp(Ac- <i>ptsc</i>)(PPh ₃)] (4)
CCDC No.	1525515	1525516
Empirical formula	C ₃₀ H ₃₂ Cl ₇ N ₃ PRuS	C ₃₃ H ₃₂ N ₃ PRuS
Formula weight	846.83	634.71
Temperature	293 K	293 K
Wavelength	0.71073 Å	0.71073 Å
Crystal system	Monoclinic	Monoclinic
Space group	P 2 ₁ /c	P 2 ₁ /c
a	15.5078(6) Å	13.5872(3) Å
b	8.1447(3) Å	11.6120(2) Å
c	29.4236(10) Å	18.5182(5) Å
α	90.0°	90°
β	93.075(3)°	99.189(2)°
γ	90.0°	90°
Volume	3711.1(2) Å ³	2884.20(12) Å ³
Z	4	4
Calculated density	1.516 Mg/m ³	1.462 Mg/m ³
Absorption coefficient	1.051 mm ⁻¹	0.699 mm ⁻¹
F(000)	1708.0	1304.0
Crystal size	0.18 x 0.18 x 0.08 mm	0.18 × 0.1 × 0.07 mm
Theta range for data collection	6.934 to 57.346	6.938 to 57.284
Limiting indices	-20 ≤ h ≤ 20, -10 ≤ k ≤ 10, -37 ≤ l ≤ 38	-17 ≤ h ≤ 17, -14 ≤ k ≤ 15, -24 ≤ l ≤ 23
Reflections collected / unique	80452/ 8840 [R(int) = 0.0769]	64094 /6709 [R(int) = 0.0484]
Completeness to theta	24.66° 99.59%	24.66° 99.63 %
Absorption correction	Semi-empirical from equivalents	Semi-empirical from equivalents
Max. and min. transmission	1.00000 and 0.72409	1.00000 and 0.81326
Refinement method	Full-matrix least-squares on F ²	Full-matrix least-squares on F ²
Data / restraints / parameters	8840/24 / 445	6709/0/352
Goodness-of-fit on F ²	1.070	1.059
Final R indices [I > 2σ(I)]	R ₁ = 0.0598, wR ₂ = 0.1104	R ₁ = 0.0376, wR ₂ = 0.0845
R indices (all data)	R ₁ = 0.0899, wR ₂ = 0.1200	R ₁ = 0.0518, wR ₂ = 0.0911
Largest diff. peak and hole	0.83 and -0.79 e·Å ⁻³	0.51 and -0.39 e·Å ⁻³

Table 2. Selected bond lengths (Å) and angles (°) for Complex 2 and Complex 4

Bond lengths	Complex 2	Bond lengths	Complex 4
Ru(1)—S(1)	2.3651(10)	Ru(1) — S(1)	2.3522(7)
Ru(1) —P(1)	2.3105(10)	Ru(1) — P(1)	2.2847(7)
Ru(1) —N(3)	2.145(3)	Ru(1) — N(1)	2.137(2)
Ru(1) —C(6)	2.157(4)	Ru(1) — C(35)	2.157(3)
Ru(1) —C(7)	2.200(4)	Ru(1) — C(36)	2.166(3)
Ru(1) —C(8)	2.208(4)	Ru(1) — C(37)	2.204(3)
Ru(1) —C(9)	2.202(4)	Ru(1) — C(38)	2.194(3)
Ru(1) —C(10)	2.160(4)	Ru(1) — C(39)	2.197(3)
Bond Angles	Complex 2	Bond Angles	Complex 4
P(1)—Ru(1) — S(1)	92.92(3)	P(1) —Ru(1) —S(1)	91.26(2)
N(3) —Ru(1) —S(1)	81.04(8)	N(1) —Ru(1) —S(1)	80.36(6)
N(3) —Ru(1) —P(1)	95.06(8)	N(1) —Ru(1) —P(1)	95.04(6)
N(3) —Ru(1) —C(6)	155.01(16)	N(1) —Ru(1) —C(35)	155.76(12)
N(3) —Ru(1) —C(7)	117.48(15)	N(1) —Ru(1) —C(36)	144.52(13)
N(3) —Ru(1) —C(8)	95.45(15)	N(1) —Ru(1) —C(37)	108.27(13)
N(3) —Ru(1) —C(9)	107.06(17)	N(1) —Ru(1) —C(38)	96.90(12)
N(3) —Ru(1) —C(10)	143.02(18)	N(1) —Ru(1) —C(39)	118.58(12)
C(6) —Ru(1) —S(1)	121.60(15)	C(35) —Ru(1) —S(1)	122.06(11)
C(6) —Ru(1) —P(1)	94.18(15)	C(35) —Ru(1) —P(1)	93.61(10)
C(6) —Ru(1) —C(7)	37.69(18)	C(35) —Ru(1) —C(36)	36.79(14)
C(6) —Ru(1) —C(8)	62.27(18)	C(35) —Ru(1) —C(37)	62.18(14)
C(6) —Ru(1) —C(9)	62.8(2)	C(35) —Ru(10)—C(38)	61.65(14)
C(6) —Ru(1) —C(10)	37.85(19)	C(35) —Ru(1) —C(39)	37.32(14)
C(7) —Ru(1) —S(1)	154.85(13)	C(36) —Ru(1) —S(1)	93.97(10)
C(7) —Ru(1) —P(1)	101.59(14)	C(36) —Ru(1) —P(1)	120.20(11)
C(7) —Ru(1) —C(8)	36.82(18)	C(36) —Ru(1) —C(37)	37.70(15)
C(7) —Ru(1) —C(9)	62.30(19)	C(36) —Ru(1) —C(38)	61.84(15)
C(8) —Ru(1) —S(1)	131.21(14)	C(36) —Ru(1) —C(39)	62.04(14)
C(8) —Ru(1) —P(1)	135.71(14)	C(37) —Ru(1) —S(1)	99.35(12)
C(9) —Ru(1) —S(1)	97.18(14)	C(37) —Ru(1) —P(1)	155.64(10)
C(9) —Ru(1) —P(1)	156.83(15)	C(38) —Ru(1) —S(1)	133.21(14)
C(9) —Ru(1) —C(8)	37.17(18)	C(38) —Ru(1) —P(1)	135.27(14)
C(10) —Ru(1) —S(1)	92.10(15)	C(38) —Ru(1) —C(37)	36.86(16)
C(10) —Ru(1) —P(1)	121.67(17)	C(38) —Ru(1) —C(39)	36.83(15)
C(10) —Ru(1) —C(7)	62.81(19)	C(39)—Ru(1) —S(1)	156.01(10)
C(10) —Ru(1) —C(8)	62.26(19)	C(39) —Ru(1) —P(1)	100.85(11)
C(10) —Ru(1) —C(9)	37.44(19)	C(39) —Ru(1) —C(37)	62.09(15)

DNA binding studies

Addition of CT-DNA to ligands (**HL**¹-**HL**⁴) and the complexes (**1-4**), a increase in the molar absorption was observed (Fig. 3 and Fig.S17). The absorption spectra of the complexes at constant concentration (10 μM) in the presence of different concentrations of CT-DNA (5–50 μM). The absorption spectra of the ligand (**HL**¹-**HL**⁴) mainly consist of only one resolved band. The absorption spectra of ligands (**HL**¹-**HL**⁴) showed one resolved band in their absorption spectra at 243 nm, 245 nm, 260 nm and 249 nm (intraligand transition) respectively. While increasing the concentration of DNA all the ligand exhibited hyperchromic red shift of 10 nm (A = 0.9008–1.8150), 10 nm (A = 0.5256–1.3154), 1nm (A = 0.2367–1.5429) and 8 nm (A = 0.2783–1.3145).Whereas, the absorption spectra of complex **1** consist of one resolved band centred at 259 nm (intraligand transition). As the DNA concentration is increased, hyperchromism (A = 0.2599–2.0788) with a blueshift of 1 nm (up to 258 nm) was observed. The spectra of complex **2** consist of one resolved band centred at 251 nm (intraligand transition). As the DNA concentration is increased, hyperchromism (A = 0.1042–1.7081) with a redshift of 4 nm was observed in the intraligand band. The spectra of complex **3** consist of one resolved band centred at 260 nm (intraligand transition). As the DNA concentration is increased, hyperchromism (A = 0.1290–1.4745) with a blueshift of 2 nm was observed in the intraligand band. Complex **4** exhibited hyperchromism in the intraligand band at 263 nm (A = 0.2057–1.0546) with 4 nm blue shift. The observed hyperchromic effect with a blue and red shift has suggested which has been suggested to reside primarily at the outer electrophilic coat of CT DNA^{51,52} predominantly *via* electrostatic interaction with the negatively charged deoxyribose- phosphate backbone.

To identify the quantitative comparison of the DNA binding affinities, we obtained the intrinsic binding constants, K_b , of the ligands and complexes for binding with calf thymus (CT DNA) by using the Stern Volmerequation :

$$[DNA]/(\epsilon_a - \epsilon_f) = [DNA]/(\epsilon_b - \epsilon_f) + 1/K_b(\epsilon_b - \epsilon_f)$$

where [DNA] is the concentration of DNA in base pairs, ϵ_a is the apparent extinction coefficient obtained by calculating $A_{obs}/[complex]$, ϵ_f corresponds to the extinction coefficient of the complex in its free form, and ϵ_b refers to the extinction coefficient of the complex in the bound form. Each set of data, when fit to the above equation, gives a straight line with a slope of $1/(\epsilon_b - \epsilon_f)$ and a y intercept of $1/K_b(\epsilon_b - \epsilon_f)$, and K_b was determined from the ratio of the slope to intercept (Fig.3 and Table. 3). The intrinsic binding constants, K_b , obtained for the complexes follow the order **2**>**3**>**4**>**1**, suggesting that the complexes are

involved in DNA binding. All the complexes showed better binding ability compared to that of their corresponding ligands.

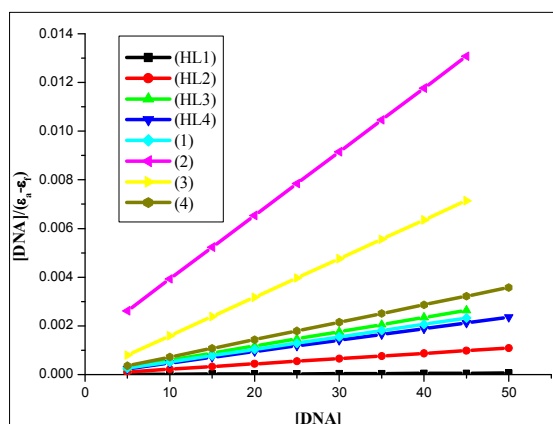


Fig.3. Plot of $[DNA]/\{\epsilon_a - \epsilon_f\}$ for ligand (HL^1 - HL^4) and complexes (1- 4).

Table 3. The binding constant K_b , for the interactions of ligands and complexes with CT-DNA

Complex	K_b/M^{-1}
HL^1	0.83×10^5
HL^2	1.63×10^5
HL^3	2.10×10^5
HL^4	2.35×10^5
1	3.71×10^5
2	1.96×10^6
3	9.52×10^5
4	5.36×10^5

Ethidium Bromide Displacement Assay

Further, the binding ability of the ligands and complexes with the CT-DNA has been confirmed by Ethidium Bromide (EB) displacement studies (Fig. 5 and Fig.S18). Ethidium Bromide competitive binding studies using ligands and new ruthenium(II) complexes (**1-4**) as

quenchers may give further information about the binding of them to DNA. The quenching extent of fluorescence of EB bound to DNA is used to determine the extent of binding of metal complexes to DNA. Upon the addition of ligands and complexes (**1-4**) (0-50 μM) to CT DNA pre-treated with EB in a 5% DMF/5 mM Tris-HCl/50 mM NaCl buffer at pH 7.2, the emission intensity at 607- 609 nm of DNA-bound EB decreases. Based on the classical Stern-Volmer equation the quenching constant has been analysed (Fig.5).

$$I_0/I = K_{sv}[Q] + 1$$

From a plot of the observed intensities against the complex concentration, the values of the apparent DNA binding constant (K_{app}) were calculated using the equation⁵³

$$K_{EB} [EB] = K_{app}[\text{complex}]$$

Where [complex] is the value at 50% reduction in the fluorescence intensity of EB, K_{EB} ($1.0 \times 10^7 \text{ M}^{-1}$) is the DNA binding constant of EB, [EB] is the concentration of Ethidium Bromide (EB) (10 μM). K_{app} values are found in Table 4. From these experimental data, it is inferred that the complex **2** replaces the EB more effectively than other complexes. From this observation, it may conclude that all the complexes can bind to DNA through the intercalation mode.

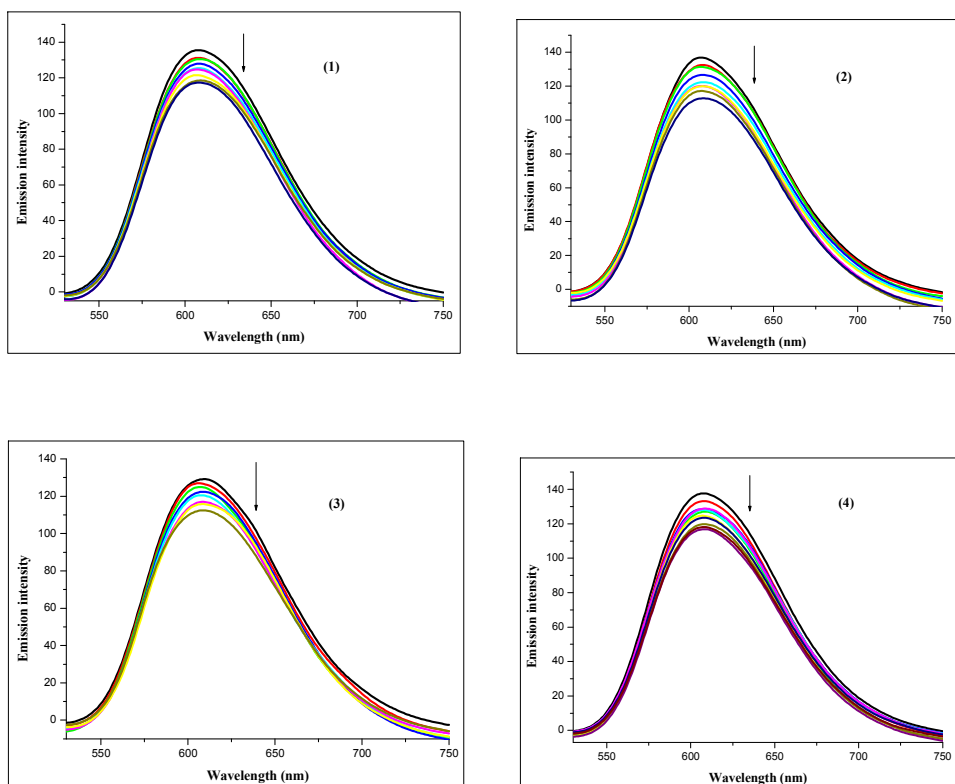


Fig.4. The emission spectra of the DNA–EB system ($\lambda_{exc} = 515 \text{ nm}$, $\lambda_{em} = 550\text{--}750 \text{ nm}$), in the presence of complexes(1-4). $[\text{DNA}] = 10 \mu\text{M}$, $[\text{Complex}] = 0\text{--}50 \mu\text{M}$, $[\text{EB}] = 10 \mu\text{M}$. The arrow shows the emission intensity changes upon increasing complex concentration.

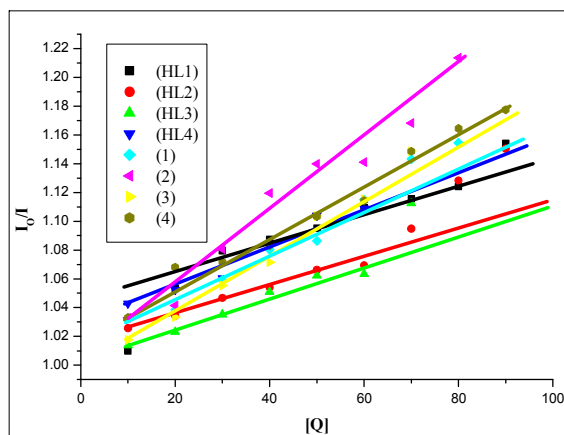


Fig.5. Stern–Volmer plots of the EB–DNA fluorescence titration for ligands and complexes

Table 4. K_{sv} , K_{app} values for the interactions of ligands and complexes with CT-DNA+EB

Complex	K_{sv}/M^{-1}	K_{app}/M^{-1}
HL ¹	1.47×10^3	1.56×10^6
HL ²	1.49×10^3	1.62×10^6
HL ³	1.44×10^3	1.58×10^6
HL ⁴	1.45×10^3	1.50×10^6
1	1.85×10^3	1.53×10^6
2	2.50×10^3	1.51×10^6
3	2.16×10^3	1.57×10^6
4	1.75×10^3	1.50×10^6

DNA cleavage study

To assess the DNA cleavage ability of the free ligands and ruthenium(II) complexes, supercoiled (SC) pBR322 DNA was incubated with complexes and ligands in 5 mM TrisHCl/50mM NaCl buffer at pH 7.2 for 2 h without addition of a reductant. Upon gel

electrophoresis of the reaction mixture, a DNA cleavage was observed (Fig. 6). The relatively fast migration is the intact supercoil form (Form I) and the slower migration is the open circular form (Form II), which was generated from supercoiled when scission occurred on its one strand.^{54,55} The intensity of supercoiled SC (Form I) diminished and partly converted to nicked form NC (Form II) by ligands (**HL**¹-**HL**³) and by complexes (**1-4**). Whereas in ligand (**HL**⁴) the intensity of supercoiled SC (Form I) increased and partly converted to nicked form NC (Form II). The intensity of the NC (Form II) band increases, whereas the production of linear form LC (Form III) of DNA diminished. It is obvious that the ligands and ruthenium(II) complexes has the ability to cleave the supercoiled plasmid DNA and this cleavage system does not require the addition of any external agents.

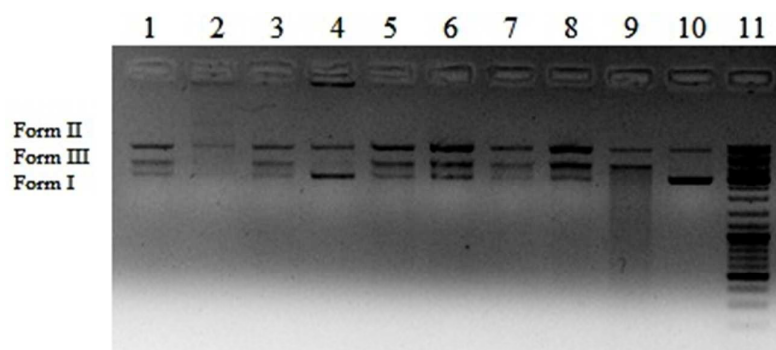


Fig. 6. Gel electrophoresis diagram showing the cleavage of supercoiled pBR322 DNA (100ng) by ligands and complexes in 5% DMSO and 95% 5 mM Tris-HCl/50 mM NaCl buffer at pH 7.2 and 37 °C with an incubation time of 2 h. Lane 1-4: Ligands (**HL**¹-**HL**⁴), Lane 5-8: Complexes (**1-4**), Lane 9: buffer+plasmid, Lanes 10: plasmid alone, and Lane 11: DNA ladder.

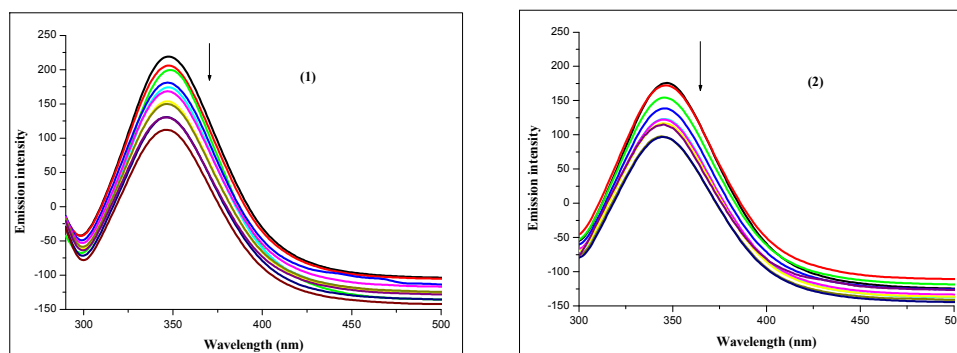
Protein binding studies

Tryptophan quenching measurements

The majority of intrinsic fluorescence of BSA when excited at 295 nm is provided by tryptophan residues alone and other amino acid residues like tyrosine and phenylalanine contribute to fluorescence only weakly.⁵⁶ In order to determine the protein binding affinity of the complexes, tryptophan quenching experiments were carried out by adding the complexes in increasing concentration (5–50 μ M) to BSA (10 μ M) at room temperature and following the decrease in fluorescence intensities. Generally, fluorescence quenching can be illustrated by the well-known Stern–Volmer equation:⁵⁷

$$I_0/I_{\text{corr}} = 1 + K_{\text{sv}} [Q]$$

where I_0 and I are the fluorescence intensities of BSA in the absence and presence of the complexes respectively, K_{sv} is the Stern–Volmer quenching constant, $[Q]$ is the concentration of the quenching complex. The value of K_{sv} obtained as a slope of the linear plot of I_0/I vs. $[Q]$ (Fig. 8). On increasing the concentration of the ligands and complexes (Fig. 7 and Fig. S19), uniform decrease in the fluorescence intensity by blue shift in ligands (HL^1 - HL^4) with 2 nm, complexes (**1**and**3**) with 3 nm and 1 nm respectively, also red shift in complex **2** with 1 nm and the complex **4** with no shift was detected, which is due to the increase in hydrophobicity of the microenvironment around tryptophan site in the protein.⁵⁸ Also, the linear fit obtained for Stern–Volmer quenching (Table. 5) analysis represents a single quenching mechanism for all the complexes. However binding affinity of complexes with BSA proportionately followed with binding ability observed for DNA binding with complexes, **2>3>4>1**. In order to investigate further whether the quenching mechanism is static or dynamic, the quenching of tryptophan emission of BSA was studied at room temperature. The absorption intensity of BSA was increased with the addition of the complexes (**1-4**) (Fig. S20). The increasing intensity in the absorbance spectra for BSA + complexes indicate the interaction of the complexes with BSA.⁵⁹ It is well known that dynamic quenching only affects the excited state of fluorophore and does not change the absorption spectrum. However, the formation of non-fluorescence ground-state complex induced the change in the absorption spectrum of fluorophore. Thus, possible quenching mechanism of fluorophore-quencher (BSA) by the complexes was found as static quenching.⁶⁰



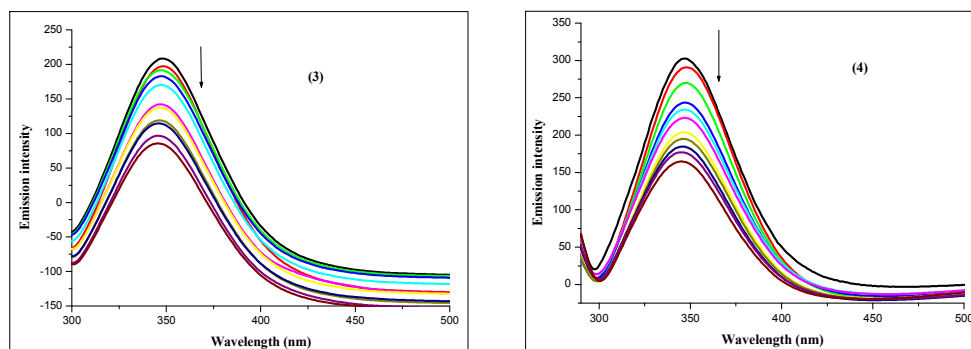


Fig.7. The emission spectrum of BSA (10 μM ; $\lambda_{\text{exc}} = 278 \text{ nm}$; $\lambda_{\text{emi}} = 347 \text{ nm}$) in the presence of increasing concentration of complexes (0 – 50 μM). The arrow shows the emission intensity changes upon increasing complexes concentration.

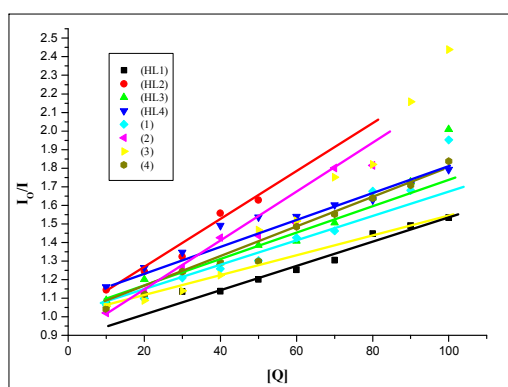


Fig. 8. Stern–Volmer plot

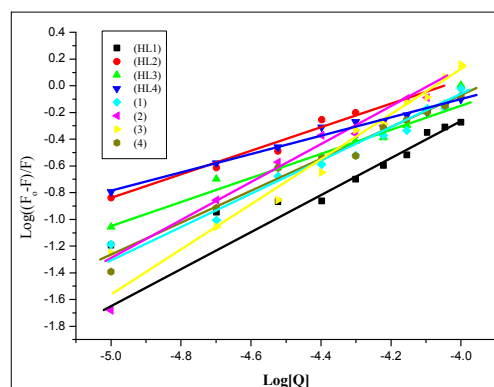


Fig.9. Scatchard plot

Determination of binding parameters and binding force

When static quenching interaction occurs, if it is assumed that the complex binds independently to a set of equivalent binding sites in BSA, the binding parameters can be determined according to the Scatchard equation:⁶¹

$$\log [(F_0 - F)/F] = \log K_b + n \log [Q]$$

where K_b is the binding constant for the binding of the complex with BSA and n is the number of binding sites per BSA molecule. By fitting the linear plot of $\log(F_0 - F)/F$ vs. $\log[Q]$ (Fig. 9, Table 5) at room temperature, the K_b values for the ligands (**HL**¹–**HL**⁴) and complexes (**1**–**4**) were calculated, which confirm that Ru(II) complexes having a large hydrophobic area can interact efficiently than ligands with BSA through a static pathway. Also, the value of n (1.1–1.6), which is approximately equal to 1, indicates that the binding site in BSA is unique and accessible by the complexes.⁶² Synchronous fluorescence spectral

study was used to obtain information about the molecular environment in the vicinity of the fluorophore moieties of BSA.⁶³ Synchronous fluorescence spectra showed tyrosine residues of BSA only at the wavelength interval $\Delta\lambda$ 15 nm whereas tryptophan residues of BSA at $\Delta\lambda$ of 60 nm (Fig. 10 and Fig. S21). While increase the concentration of complexes (0–50 μM) added to BSA (10 μM), a decrease in the fluorescence intensity in the tryptophan emission maximum is observed for all the complexes (Fig. 10). In contrast, the emission intensity of tyrosine residue increases without any change in the wavelength of emission. These observations indicate that the test compounds did not affect the microenvironment of tyrosine residues during the binding process significantly.

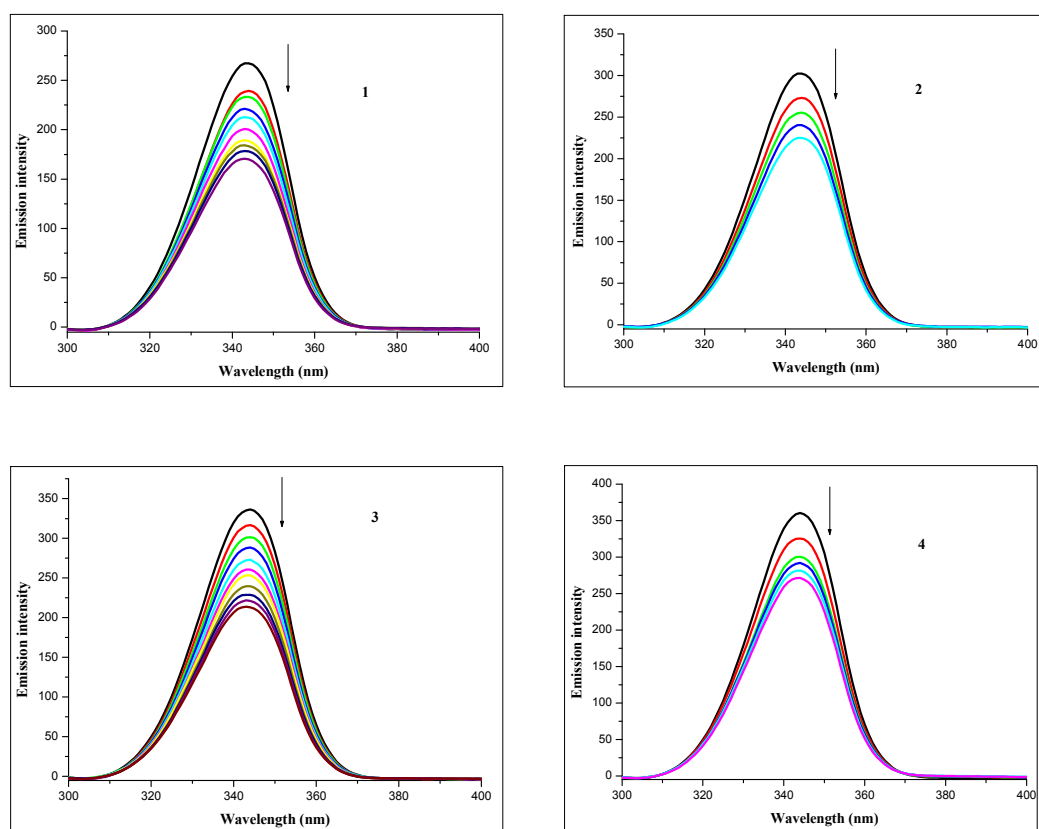


Fig. 10. Synchronous spectra of BSA (10 μM) in the presence of increasing concentration of complexes 1-4 for a wavelength difference of $\Delta\lambda = 60$ nm. The arrow shows the emission intensity changes upon increasing concentration of complex.

Table 5. Quenching constant (K_{sv}), binding constant (K_{bin}) and number of binding sites (n) for the interactions of complexes (1–4) with BSA

Complex	K_b/M^{-1}	K_{sv}/M^{-1}	n
HL ¹	0.23×10^4	5.54×10^3	0.92
HL ²	0.63×10^4	1.28×10^3	0.93
HL ³	0.50×10^4	8.84×10^3	0.95
HL ⁴	0.03×10^4	6.42×10^3	0.67
1	3.44×10^4	9.17×10^3	1.16
2	3.97×10^6	1.14×10^3	1.61
3	1.12×10^6	1.51×10^3	1.49
4	9.32×10^4	8.62×10^3	1.25

HSA-binding studies

The fluorescence titrations of the Ru(II) complex with HSA were carried out in Tris-HCl buffer of pH 7.2. Fluorescence spectroscopy is an effective method used to explore the interaction between small molecules and biomacro-molecules. The fluorescence emission spectra of HSA recorded in the range of 300–500 nm by exciting the HSA at 280 nm at various concentration of the Ru(II) complex are shown in Fig.11. The HSA shows a strong fluorescence emission with a peak at 342–343 nm, while ligands and the complexes has no intrinsic fluorescence under the present experiment conditions. The fluorescence intensities of the HSA decreased continually with increasing concentration of the complexes, accompanied with a blue shift (from 342 to 340 nm), indicating that the binding of the complexes to HSA changed the local microenvironment around the Trp-214 residue in HSA, and concomitantly the tertiary structure of the HSA. Commonly, fluorescence quenching can be described by the following Stern–Volmer equation:⁶⁴

$$I_0/I = 1 + K_{sv} [Q]$$

where I_0 and I are the fluorescence intensities of HSA in the absence and presence of the complexes respectively, K_{sv} is the Stern–Volmer quenching constant, $[Q]$ is the concentration of the quenching complexes. The value of K_{sv} obtained as a slope of the linear

plot of I_0/I vs. $[Q]$ (Fig.12). On increasing the concentration of the ligands and complexes (Fig. 11 and Fig.S22), uniform decrease in the fluorescence intensity by blue shift in ligands (HL^1 - HL^4) and complexes (**1-4**), which is due to the increase in hydrophobicity of the microenvironment around tryptophan site in the protein. Also, the linear fit obtained for Stern–Volmer quenching (Table. 6) analysis represents a single quenching mechanism for all the complexes.

In order to investigate further whether the quenching mechanism is static or dynamic, the quenching of tryptophan emission of HSA was studied at room temperature. The absorption intensity of HSA was increased with the addition of the complexes (**1-4**) (Fig. S23). The increasing intensity in the absorbance spectra for HSA + complexes indicate the interaction of the complexes with HSA. It is well known that dynamic quenching only affects the excited state of fluorophore and does not change the absorption spectrum. However, the formation of non-fluorescence ground-state complex induced the change in the absorption spectrum of fluorophore. Thus, possible quenching mechanism of fluorophore-quencher (HSA) by the complexes was found as static quenching.⁶⁵

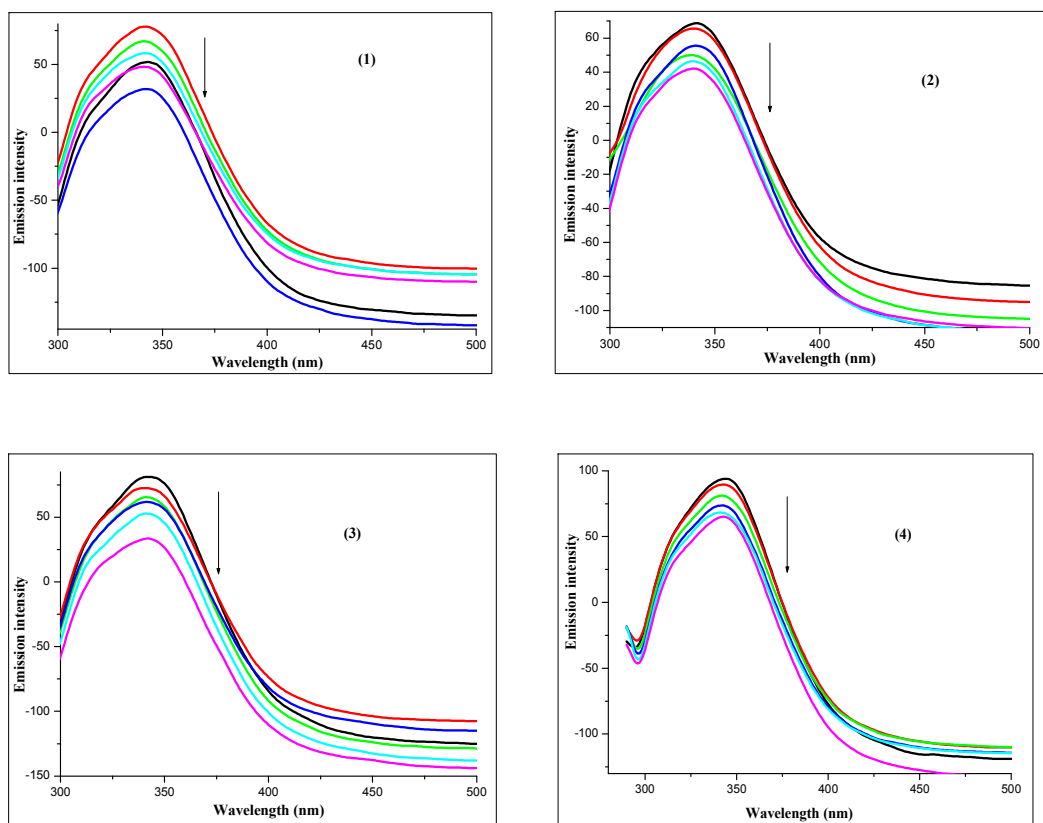


Fig. 11. The emission spectrum of HSA (10 μM ; $\lambda_{\text{exc}} = 280 \text{ nm}$; $\lambda_{\text{emi}} = 340 \text{ nm}$) in the presence of increasing concentration of complexes (0 – 50 μM). The arrow shows the emission intensity changes upon increasing complexes concentration.

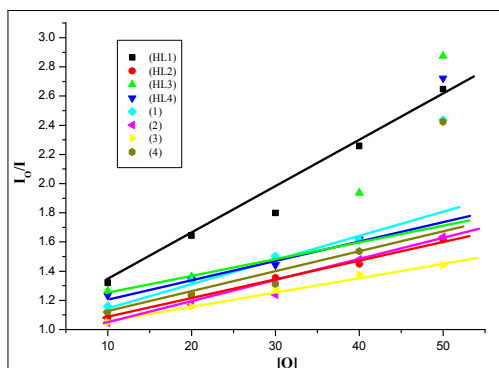


Fig. 12. Stern–Volmer plot

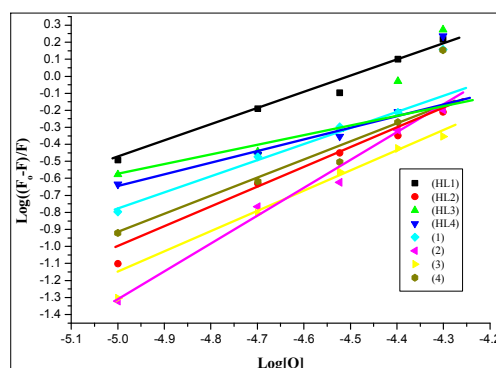


Fig. 13. Scatchard plot

Determination of binding parameters and binding force

When static quenching interaction occurs, if it is assumed that the complexes binds independently to a set of equivalent binding sites on a macromolecules, the binding parameters can be determined according to the Scatchard equation:⁶¹

$$\log [(F_0 - F)/F] = \log K_b + n \log [Q]$$

where K_b is the binding constant for the binding of the complexes with HSA and n is the number of binding sites per HSA molecule. By fitting the linear plot of $\log(F_0 - F)/F$ vs. $\log[Q]$ (Fig.13, Table 6) at room temperature, the K_b values for the ligands (**HL¹-HL⁴**) and complexes (**1-4**) were calculated, which confirm that Ru(II) complexes having a large hydrophobic area can interact efficiently than ligands with HSA through a static pathway. Also, the value of n (0.9–1.5), which is approximately equal to 1, indicates that the binding site in HSA is unique and accessible by the complexes. Herein, binding affinity of complexes with BSA proportionately followed with HSA, **2>3>4>1**.

Table 6. Quenching constant (K_{sv}), binding constant (K_{bin}) and number of binding sites (n) for the interactions of complexes (**1-4**) with HSA

Complex	K_b/M^{-1}	K_{sv}/M^{-1}	n
---------	---------------------	------------------------	-----

HL¹	2.70×10^4	3.26×10^4	0.98
HL²	1.39×10^5	1.28×10^5	1.39
HL³	8.93×10^4	3.79×10^4	1.12
HL⁴	3.72×10^4	3.25×10^4	1.05
1	1.87×10^5	2.82×10^4	1.22
2	4.27×10^6	1.48×10^4	1.58
3	6.74×10^5	2.90×10^4	1.36
4	4.49×10^5	1.00×10^4	1.38

Anticancer evaluation of compounds using MTT assay

To evaluate the cytotoxic effect of the ligands and complexes on the cell viability of MCF-7 cancer cells and HaCaT (human immortalized, but 'non-cancerous') cells, MTT assay was performed. The results from the triplicate MTT assays showed a significant inhibitory effect for all the complexes (Fig.14). On the basis of this assay, complex **2** exhibited the highest cytotoxic activity or lower IC₅₀ value followed by complex **3**, whereas complexes **4** and **1** displayed less activity. However ligands displayed no significant cytotoxic activity against MCF-7 cells. The IC₅₀ values for the complexes **1**, **2**, **3** and **4** are 27.27 μM (16.23±94 μg/ml), 10.67 μM (6.5±0.19 μg/ml), 11.13 μM (7.7±0.42 μg/ml) and 17.85 μM (11.13±0.24 μg/ml) respectively. From the results obtained, we found that all the complexes (**1-4**) showed an enhanced growth inhibitory effect than the recognized drug *cisplatin* with the IC₅₀ value of 23.7 μM against MCF-7 cell lines. Among the four complexes, **2** and **3** are the most effective complexes against the MCF-7 cell line. Hence, the complexes **2** and **3** have been taken for apoptotic morphological investigation. While comparing the results of complexes reported by Ferriet *al*, our complexes showed good cytotoxicity against the MCF-7 and other cancer cell lines.^{66, 67}

Further anti-cancer drugs with minimal side effects on normal cells are highly desirable for therapeutic purposes.⁶⁸ Hence, the current study also addressed the question of whether synthesized complexes mediated suppression of cell viability was selectively to cancer cells. Non-cancerous normal human keratinocyte line (HaCaT) or Human immortalized but non cancerous cell line (HaCaT) is a spontaneously transformed aneuploid immortal keratinocyte

cell line from adult human skin.^{69,70} HaCaT cells are utilized for their high capacity to differentiate and proliferate *in vitro*.⁷¹ Their use in research allows for the characterization of human keratinocyte using a model that is reproducible and addresses issues such as short culture lifespan and variations between cell lines that would otherwise be encountered. These cells have allowed the characterization of several processes, such as their utilization as a model system for vitamin D₃ metabolism in the skin.⁷² Cytotoxicity study against human immortalized, but 'non-cancerous' cell line (HaCaT) indicated that the complexes (1-4) possess less cytotoxic activity against 'non-cancerous' cells (Fig. 15). Agents that are capable of inducing selective apoptosis of cancer cells, without causing much harm to normal cells, have received considerable interest in the development of novel cancer chemotherapeutic drugs.⁷³ We found that concentrations of complexes (1-4) were cytotoxic to human breast cancer MCF7 cells but failed to induce apoptosis in HaCaT cells. These results suggest that complexes (1-4) possess anti-cancer activities in human breast cancer cells without cytotoxic effects against human 'non-cancerous' cells (HaCaT). Thus, these complexes extracts can be evaluated further for potential anticancer properties.

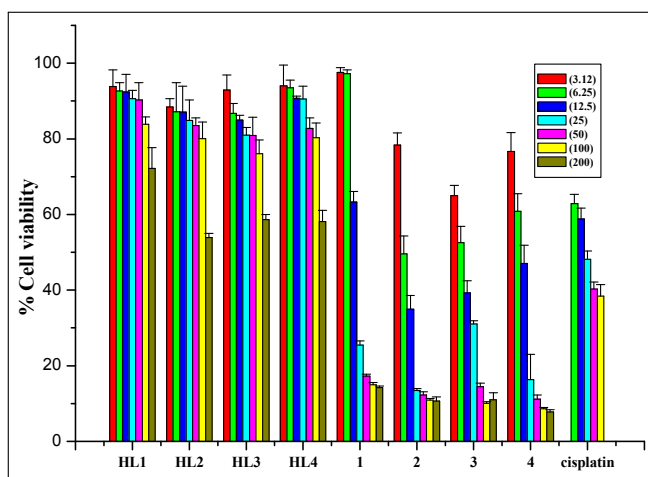


Fig.14. The % Cell viability for the ligands, complexes and *cisplatin*. MTT(3-(4,5-dimethylthiazol-2-yl)-2,5-diphenyltetrazoliumbromide) assay.

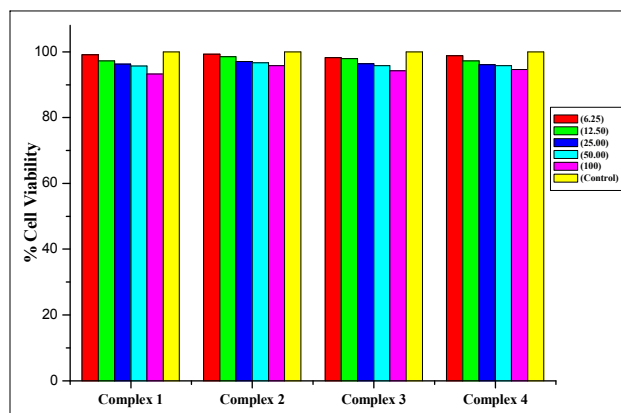
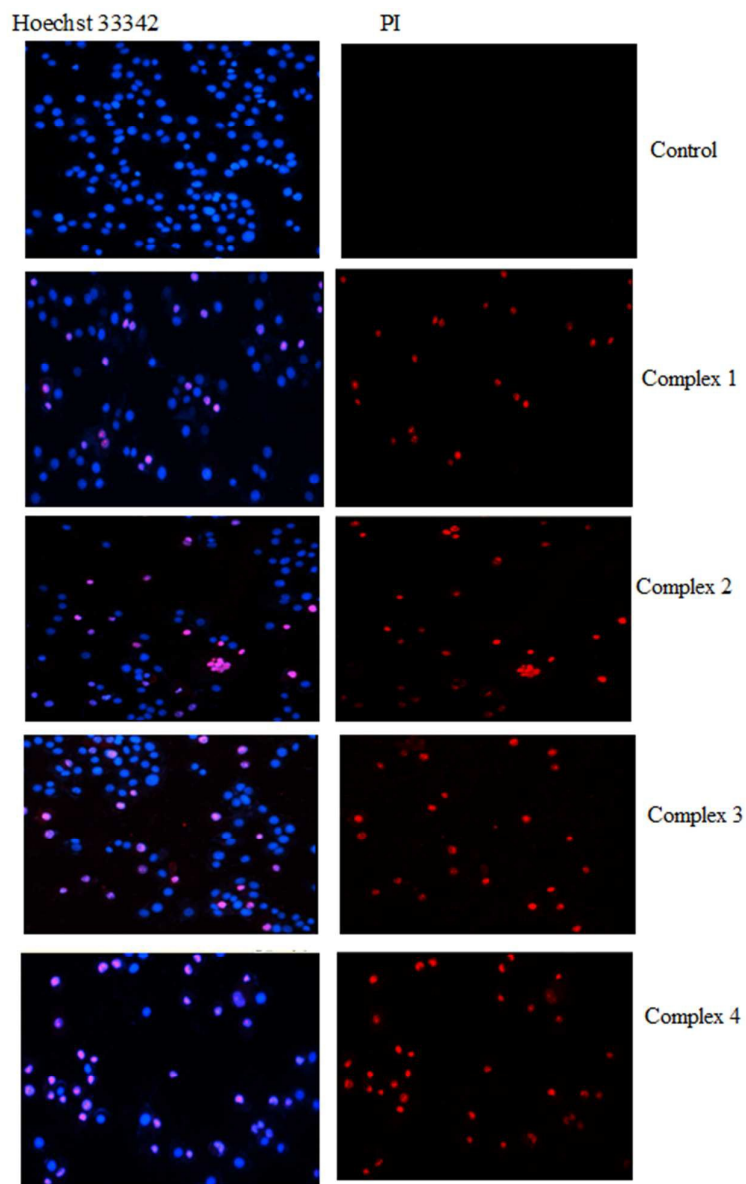


Fig. 15. The % Cell viability for the ligands, complexes against HeCaT cells (non-cancerous cell).

Morphological changes of nucleus with Hoechst 33342/PI Staining

Nuclear fragmentation is one of the prime features of apoptotic cell death. To investigate the cell death by apoptosis and changes in the nuclear morphology, DNA binding dyes Hoechst and PI were used to investigate nucleus morphology of the control and treated cells (Fig.16). Hoechst is permeable to cell membrane and typically used to stain the nucleus of live/dead cells. Hoechst binds to the minor groove of double strand DNA preferably at AT rich regions and stains nucleus in blue colour. PI is usually used to identify the dead cells and its membrane impermeability and gets excluded from viable cells. PI binds to DNA by intercalating between the bases without any sequence preference and gives red colour at respective wavelength.

Morphological analysis of MCF-7 cell nuclei with Hoechst 33342 and PI staining after treating the cells with complexes **2** and **3** at IC_{50} concentration at 24 h, displayed morphological alterations compared to untreated control cells. As shown in Fig.17, the control cells stained with Hoechst 33342 dye with blue fluorescence represents all cells are live and healthy, while the treated cells stained with Hoechst 33342 and propidium iodide resulted in a red fluorescence or pink in the merged photo representing dead cells (late apoptosis or necrosis), could be clearly visualized due to toxicity of the drugs and cell membrane disruption.



Complex 2 (IC₅₀ concentration) Complex 3 (IC₅₀ concentration)

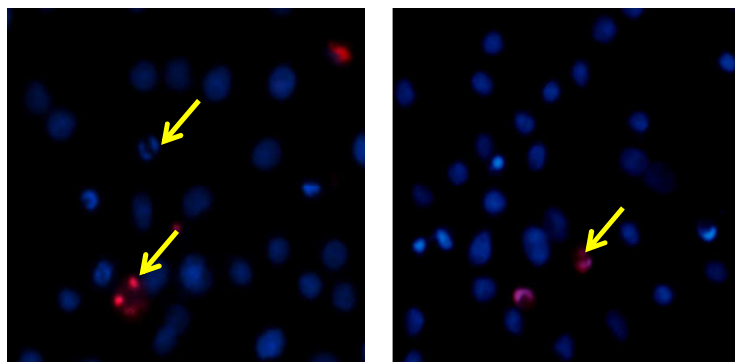


Fig.16. Morphological changes of MCF-7 cells after treatment with IC₅₀ concentration of the compounds. The cells were double stained with Hoechst 33342 and PI. The nuclei of the cells

were visualized using an inverted fluorescent microscope (100 X). Apoptotic/necrotic cells displayed red (or pink) fluorescence while live cells displayed blue fluorescence. Yellow arrows indicate nuclear condensation and nuclear fragmentation.

Apoptotic morphological observation of treated MCF-7 Cells using phase contrast inverted microscope

The apoptogenic property of the active complexes (**2** and **3**) was investigated through morphological changes in MCF-7 human breast cancer cells. Apoptotic cells displayed typical common features such as cell shrinkage, rounding and membrane blebbing. These distinctive typical form of morphological changes in apoptotic cells are widely used for the identification and quantification of apoptosis.⁷⁴ Thus, determination of the morphological changes to define apoptosis was visualised using inverted phase contrast microscope. After incubation with tested compounds for 24 h, morphological alterations in MCF-7 cells were observed (Fig.17) in comparison to control cells. Visualization of the control (untreated) cells showed that the cells maintained their original morphology. Most of the control cells were adherent to the tissue culture dishes. In contrast, exposure of MCF-7 breast cancer cell treated with complexes **2** and **4** for 24 h revealed typical apoptotic features such as rounding, shrinkage, membrane blebbing, and losing contact with adjacent cells. Therefore, the exposure of MCF-7 cells to both complexes can induce the apoptotic morphology changes, which become more remarkable as the dose of the tested complexes was increased.

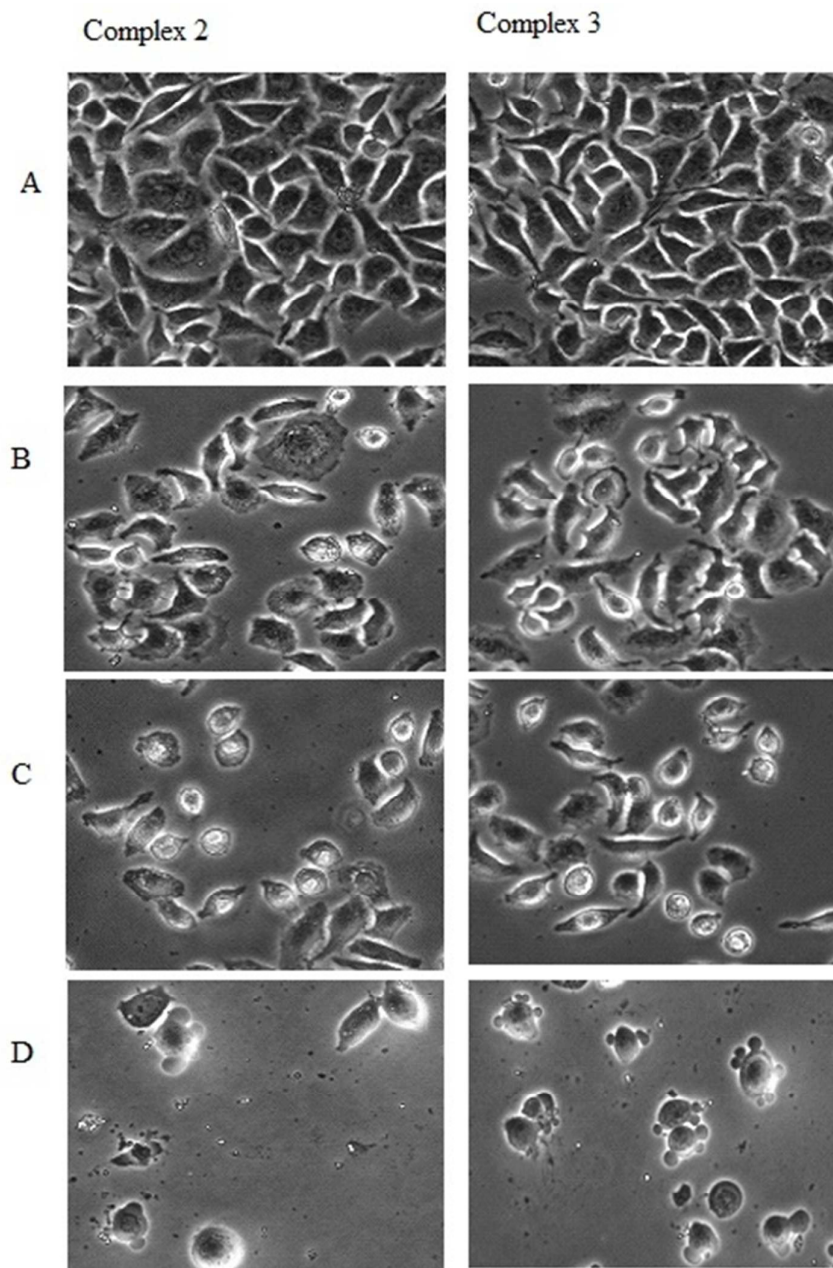


Fig.17. Morphological changes induced by complex 2 and complex 3 treatment in breast cancer cells. MCF-7 cells were treated with complex 2 (3 μ g/ml,6 μ g/ml and 12 μ g/ml) and complex 3(3.5 μ g/ml,7 μ g/ml and 14 μ g/ml) for 24h, and the cells were visualized under phase-contrast microscopy (100 X) to investigate the morphological alteration. Apoptosis characteristic such as shrinkage, rounding of the cell shape and membrane blebbing were observed in both compounds. In this Fig., (A) shows the control (untreated) cells and (B, C, D) shows the MCF-7 treated cells with different concentration as indicated above.

Apoptosis analysis with Annexin V-FITC /PI

Additional evidence for the occurrence of apoptosis in MCF7 cells was achieved through the double staining with propidium iodide, which stains the nuclei of dead cells representing the late apoptosis (Annexin-V-FITC+, PI+) or necrosis (Annexin-V-FITC-, PI+), and Annexin V-FITC, which binds to phosphatidylserine in of outer membrane representing the early apoptosis (Annexin-V-FITC+, PI-). As shown in Fig. 18, there is a shift from viable to early apoptosis and to late apoptosis/necrosis as the dose increases. These findings showed that the cytotoxic effect of both the complexes towards MCF7 cells was mediated via the induction of apoptosis.

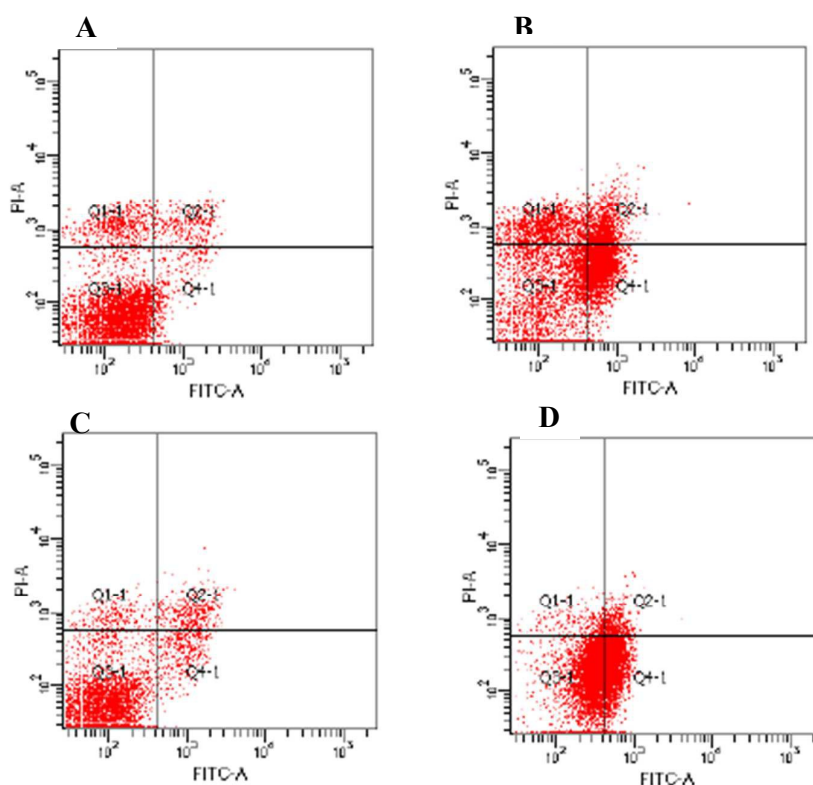


Fig.18. Apoptosis evaluation of MCF-7 cells treated with **3** and **2** compounds. A and B represent treated cells with 7 $\mu\text{g/ml}$ and 14 $\mu\text{g/ml}$ of **3** after 24h incubation, respectively. C and D represent treated cells with 6 $\mu\text{g/ml}$ and 12 $\mu\text{g/ml}$ of **2** after 24h incubation, respectively. In this Fig., Q3-1, Q4-1, Q2-1, and Q1-1 are related to live cells, early apoptosis, late apoptosis, and necrosis, respectively.

Conclusion

Four new organo-ruthenium complexes were synthesized and characterized by various analytical and spectroscopic techniques. The structure of the complexes **2** and **4** were confirmed X-ray crystallography. CT- DNA and protein binding studies have been carried

out for all the ligands and complexes. The complexes possess higher activity as compared with their corresponding ligands. In supercoiled plasmid DNA cleavage study showed that the complexes have the ability to cleave the DNA without the addition of any external agents. However, the order of binding affinity of the complexes is no longer been followed in DNA cleavage and thus currently it is not possible to correlate the binding affinity of the complexes with cleavage ability. The BSA interaction potential of the complexes was determined by fluorescence quenching experiments and indicates a strong interaction between the fluorophore and quencher with static quenching mechanism. *In vitro* cell proliferation assay supported their notable cytotoxic nature against the MCF7 cell line. The complexes **2** and **3**, showing better activity with lowest IC_{50} values compared to the standard *cisplatin*. Morphological analysis using inverted phase contrast microscope, Hoechst 33342/PI dual staining procedures by fluorescence microscope, showed that complexes **2** and **3** were able to trigger cell death of human MCF-7 breast cancer cells through apoptosis in a dose-dependent manner. While comparing the results of CT-DNA/ BSA/ HSA binding abilities and cytotoxicity of the complexes, it is inferred that the DNA/ protein binding ability of the complexes were proportionately influenced by the cytotoxicity of the complexes which follows the order **2**>**3**>**4**>**1**. In addition, complexes **2** and **3** have the capability to induce apoptosis. The finding of the present study thus supported the use of complexes **2** and **3** in medicine for the treatment of breast cancers after further biological evaluation.

Supporting Information

Fig.s S1-S25, Table S1.

■ AUTHOR INFORMATION

Corresponding author Tel.: +91-422-2428319; Fax: +91-422-2422387.

E-mail address: rpncchemist@gmail.com (R. Prabhakaran)

ACKNOWLEDGMENTS

The author P.K. gratefully acknowledges **Department of Science and Technology (DST-SERB), New Delhi, India (No. SB/FT/CS-056-/2014 dated 12.08.2015)** for the financial support. The author R. F. acknowledges **PPP grant (PG263-2015B)** from **University of Malaya** for anticancer studies.

References

1. Jung Y.;Lippard, S. J. *Chem. Rev.***2007**, *107*(5), 1387–1407.
2. Todd, R.C.;Lippard.S. J. *Metallomics***2009**, *1*(4), 280–291.
3. Baruah, Barry, C. G.; Bierbach, U. *Curr. TopMed. Chem.* **2004**, *4*(15), 1537–1549.
4. Kelland, L.*Nat. Rev. Cancer***2007**, *7*(8), 573–584.
5. Lara, S. B.; Salassa,L.;Habtemariam, A.; Novakova,O.; Pizarro, A. M.; Clarkson,G. J. *Organometallics***2012**, *31*(9), 3466–3479.
6. Bugarcic,T.;Habtemariam,A.;Deeth,R.J.;Fabbiani,F.P.; Parsons,S.; Sadler,P.J. *Inorg. Chem.* **2009**, *48*(19), 9444–9453.
7. Fernandez,R.;Melchart,M.;Habtemariam,A.; Parsons,S.; Sadler,P. J. *Chemistry***2004**, *10*(20), 5173–5179.
8. Habtemariam,A.;Melchart,M.; Fernandez,R.; Parsons, S.; Oswald,I.D.H.;Parkin,A. J. *Med. Chem.* **2006**, *49*(23), 6858–6868.
9. Ang,W.H.; Dyson,P.J. *Eur. J. Inorg. Chem.* **2006**, *20*, 4003–4018.
10. Wang,F.Y.; Chen,H.M.; Parkinson,J.A.; Murdoch,P.D.; Sadler,P.J. *Inorg. Chem.***2002**, *41*(17), 4509–4523.
11. Kuhn,P.S.;Pichler,V.; Roller,A.;Hejl,M.;Jakupec,M.A.;Kandioller,W. *DaltonTrans.* **2015**, *44*(2), 659–668.
12. Leijen,S.; Burgers,S.A.; Baas,P.;Pluim,D.;Tibben, M.; vanWerkhoven,E. *InvestNewDrugs***2015**, *33*(1), 201–214.
13. Lentz,F.;Drescher,A.;Lindauer,A.; Henke,M.;Hilger,R. A.;Hartinger,C. G. *Anticancer Drugs***2009**, *20*(2), 97–103.
14. Novakova,O.;Kasparkova, J.;Bursova,V.;Hofr,C.;Vojtiskova,M. Chen,H. M. *Chem. Biol.***2005**, *12*(1),121–129.
15. Ang,W.H.;Casini,A.; Sava,G.; Dyson, P.J.*J.Organomet. Chem.* **2011**, *696*(5), 989–998.
16. Bergamo,A.;Masi,A.; Peacock,A.F.A.;Habtemariam, A.; Sadler,P. J.; Sava,G. *J. Inorg. Biochem.***2010**, *104*(1), 79–86.
17. Weiss, A.; Bonvin, D.; Berndsen, R.H.; Scherrer,E.; Wong,T.J.; Dyson, P.J. *Sci.Rep.***2015**, *5*, 8990.
18. Quiroga,A.G.;Ranninger, C.N.*Coord. Chem. Rev.***2004**, *248*, 119–133.
19. Takacs,Z.; Nathan,S. Animal venoms in medicine. In: Wexler P (ed) Encyclopedia of toxicology, 3rd edn. *Elsevier*, London, **2014**, 252–259.
20. Ellmore,S. *Toxicol. Pathol.***2007**, *35*, 495–516

21. Bold, R. J.; Termuhlen, P. M.; McConkey, D. J. *Surg. Oncol.* **1997**, *6*, 133–142.
22. Kamesaki, H. *Int. J. Hematol.* **1998**, *68*, 29–43.
23. Thompson, C.B. *Science*, 1995, **267**, 1456–1462.
24. Kroemer, G.; Petit, P.; Zamzami, N.; Vayssiere, J.L.; Mignotte, B. *Fed. Am. Soc. Exp. Biol. J.* 1995, **9**, 1277–1287.
25. Moongkarndi, P.; Kosem, N.; Kaslungka, S.; Luanratana, O.; Pongpan, N.; Neungton, N. *Journal of Ethnopharmacology*, **2004**, *90*, 161–166.
26. Abdel Wahab, S.I.; Abdul, A.B.; Alzubairi, A.S.; Mohamed Elhassan, M.; Mohan, S. *Journal of Biomedicine and Biotechnology*, **2009**, ID-769568, 10 pages.
27. Brown, J.M.; Attardi, L.D. *Nature Reviews Cancer*, **2005**, *5* (3), pp. 231–237.
28. Thuret, G.; Chiquet, C.; Herrag, S. *British Journal of Ophthalmology*, **2003**, *87*, 346–352.
29. Blessing, R.H. *Acta Crystallogr. Sect. A* **1995**, *51*, 33–38.
30. Sheldrick, G.M. SHELXTL Version 5.1, An Integrated System for Solving, Refining and Displaying Crystal Structures from Diffraction Data, Siemens Analytical X-ray Instruments, Madison, WI, **1990**.
31. Sheldrick, G.M. Shelxl-97, A Program for Crystal Structure Refinement Release 97-2, Institut für Anorganische Chemie der Universität Göttingen, Tammanstrasse 4, D-3400, Göttingen, Germany, **1998**.
32. Vogel, A.I. *Text Book of Practical Organic Chemistry*, Vth ed., Longman London, **1989**, 268.
33. Beckford, F.; Dourth, D.; Jr. Shaloski, M.; Didion, J.; Thessing, J.; Woods, J.; Crowell, V.; Gerasimchuk, N.; Gonzalez-Sarrias, A.; Seeram, N.P. *J. Inorg. Biochem.* **2011**, *105*, 1019–1029.
34. Su, W.; Qian, Q.; Li, P.; Lei, X.; Xiao, Q.; Huang, S.; Huang, C.; Cui, J. *Inorg. Chem.* **2013**, *52*, 12440–12449.
35. Bruce, M.I.; Windsor, N.J. *Aust. J. Chem.*, **1977**, *30*, 1601–1604.
36. Berridge, M.V.; Herst, P.M.; Tan, A.S. *Biotechnol. Ann. Rev.* **2005**, *11*, 127–152.
37. Ziegler, U.; Groscurth, P. *News Physiol. Sci.* **2004**, *19*, 124–128.
38. Bezabeh, T.; Mowat, M.R.A.; Jarolim, L.; Greenberg, A.H.; Smith, I.C.P. *Cell Death Differ.* **2001**, *8*, 219–224.
39. Rodrigues, C.; Batista, A.A.; Aucélio, R.Q.; Teixeira, L.R.; Visentin, L.C.; Beraldo, H. *Polyhedron* **2008**, *27*, 3061–3066.

40. Su, W.; Qian, Q.; Li, P.; Lei, X.; Xiao, Q.; Huang, S.; Huang, C.; Cui, J. *Inorg. Chem.* **2013**, *52*, 12440-12449.
41. Prabhakaran, R.; Renukadevi, S.V.; Karvembu, R.; Huang, R.; Mautz, J.; Huttner, G.; Subashkumar, R.; Natarajan, K. *Eur. J. Med. Chem.* **2008**, *43*, 268-273.
42. Kalaivani, P.; Prabhakaran, R.; Poornima, P.; Dallemer, F.; Vijayalakshmi, K.; Vijaya Padma, V.; Natarajan, K. *Organometallics* **2012**, *31*, 8323-8332.
43. Jouad, E.M.; Riou, A.; Allain, M.; Khan, M.A.; Bouet, G.M. *Polyhedron* **2001**, *20*, 67-74.
44. Govindaswamy, P.; Mozharivskyj, Y.A.; Kollipara, M.R. *Polyhedron*, **2004**, *23*, 1567-1572.
45. Klayman, D.L.; Scovill, J.P.; Brtosevich, J.F.; Bruce, J. *J. Med. Chem.* **1983**, *26*, 35-39.
46. Chikate, R.C.; Padhye, S.B. *Polyhedron* **2005**, *24*, 1689-1700.
47. Alomar, K.; Khan, M.A.; Allain, M.; Bouet, G. *Polyhedron* **2009**, *28*, 1273-1280.
48. Jia, G.; Meek, D. W. *Organometallics* 1991, **10**, 1444-1450
49. Abou-Hussein, A.A.; Linert, W. *Spectrochimica Acta Part A: Molecular and Biomolecular Spectroscopy* **2014**, *117*, 763-771.
50. Govindaswamy, P.; Sinha, C.; Kollipara, M.R. *J. Organomet. chem.* **2005**, *690*, 3465-3473.
51. Yang, I.V.; Thorp, H.H.; *Inorg. Chem.* **2000**, *39*, 4969-4976.
52. Stradowski, C.; Corner, H.; Currell, L.J.H.; Schutte-Frohlude, D. *Biopolymers* **1987**, *26*, 189-201.
53. Parta, A. K.; Dhar, S.; Nethaji, M.; Chakravarty, A. R. *Dalton Trans.* **2005**, 896-902.
54. Gao, E.; Sun, Y.; Liu, Q.; Duan, L. *J. Coord. Chem.* **2006**, *59*, 1295-1300.
55. Baguley, B. C.; LeBret, M. *Biochemistry* **1984**, *23*, 937-943.
56. Wang, C.X.; Yan, F.F.; Zhang, Y.X.; Ye, L. *J. Photochem. Photobiol. A*, **2007**, *192*, 23-28.
57. Lakowicz, J. R. *Springer*, New York, 3rd edn, **2006**.
58. Kragh-Hansen, U.; Hellec, F.; de Foresta, B.; le Maire, M.; Moller, J.V. *Biophys. J.* **2001**, *80*, 2898-2911.
59. Yue, Y.Y.; Chen, X. G.; Qin, J.; Yao, X. J. *Dyes Pigm.* **2008**, *79*, 176-182.
60. Liu, H.Y.; Xu, Z.H.; Liu, X.H. *Chem. Pharm. Bull.* **2009**, *57*, 1237-1242.
61. Divsalar, A.; Bagheri, M.J.; Saboury, A.; Mansoori-Torshizi, H.; Amani, M.; *J. Phys. Chem. B*, **2009**, *113*, 14035-14042.

62. Gao, H.; Lei, L.D.; Liu, J.Q.; Kong, Q.; Chen, X. G.; Hu, Z.D. *J. Photochem. Photobiol.* **2004**, *167*, 213-221.
63. Wang, N.; Ye, L.; Zhao, B.Q.; Yu, J.X. *J. Med. Biol. Res.* **2008**, *41*, 589-595.
64. Trynda-Lemiesz, L.; Keppler, B.K.; Koztowski, H. *J. Inorg. Biochem.* **1999**, *73*, 123-128.
65. Eftink, M.R.; Ghiron, C.A. *Biochemistry* **1976**, *15*, 672-680.
66. Mendoza-Ferri, M. G.; Hartinger, C. G.; Mendoza, M. A.; Groessl, M.; Egger, A. E.; Eichinger, R. E.; Mangrum, J. B.; Farrell, N. P.; Maruszak, M.; Bednarski, P. J.; Klein, F.; Jakupec, M. A.; Nazarov, A. A.; Severin, K.; Keppler, B. K.. *J. Med. Chem.* **2009**, *52*, 916-925.
67. Subarkhan, M. K. M.; Ramesh, R. *Inorg. Chem. Front.*, **2016**, *3*, 1245
68. Buolamwini, J. K. *Current Opinion in Chemical Biology* **1999**, *3(4)*, 500-509.
69. Boukamp, P.; Petrussevska, R. T.; Breitkreutz, D.; Hornung, J.; Markham, A.; Fusenig, N. E. *J. Cell Biol.* **1988**, *106*, 761-771
70. Schoop, V. M.; Mirancea, N.; Fusenig, N. E. *Journal of Investigative Dermatology* **1999**, *112 (3)*, 343-353.
71. Schurer, N.; Kohne, A.; Schliep, V.; Barlag, K.; Goerz, G. *Experimental Dermatology*, **1993**, *2 (4)*, 179-185.
72. Lehmann, B. *Journal of Investigative Dermatology* **1997**, *108 (1)*, 78-82.
73. Cotter, T. G. *Nature Reviews Cancer* **2009**, *9*, 501-507.
74. Brady, H. J. M. *Apoptosis Methods and Protocols*, Humana Press, Totowa, NJ, USA, **2004**.

